

Phosphine-Coordinated Pure-Gold Clusters: Diverse Geometrical Structures and Unique Optical Properties/Responses

Katsuaki Konishi

Abstract Synthetic techniques, geometrical structures, and electronic absorption spectra of phosphine-coordinated pure-gold molecular clusters (PGCs) accumulated over 40 years are comprehensively collected especially for those with unambiguous X-ray crystal structures available. Inspection of the electronic absorption spectra from geometrical aspects reveals that their optical properties are highly dependent on the cluster geometries rather than the nuclearity. Recent examples of unusual clusters that show unique color/photoluminescence properties and their utilization for stimuli-responsive modules are also presented.

Keywords Absorption spectrum · Chromism · Gold cluster · Optical property · Phosphine · Photoluminescence · Stimuli-responsive materials

Contents

1	Introduction	50
2	Characterization	52
3	Synthesis	52
3.1	Direct Syntheses from Gold Complex Ion or Bulk Gold	54
3.2	Post Synthesis	58
4	Geometrical Structure	61
4.1	Centered Polyhedral Clusters	64
4.2	Non-centered Polyhedral Clusters	67
4.3	<i>Exo</i> -attached Polyhedral Clusters (<i>core+exo</i> Type)	69
5	Optical Properties	71
5.1	Electronic Absorption Spectra	71
5.2	Photoluminescence	77
5.3	Gold Clusters as Stimuli-Responsive Chromic Modules	79

K. Konishi (✉)

Faculty of Environmental Earth Science and Graduate School of Environmental Science,
Hokkaido University, North 10 West 5, Sapporo 060-0810, Japan
e-mail: konishi@ees.hokudai.ac.jp

6 Concluding Remarks	81
References	81

Abbreviations

Ar	Aryl
AZS	Alizarinsulfonate
Bu	Butyl
DCM	Dichloromethane
dppb	Bis(diphenylphosphino)butane
dppe	Bis(diphenylphosphino)propane
dpph	Bis(diphenylphosphino)hexane
dppm	Bis(diphenylphosphino)methane
dppo	Bis(diphenylphosphino)octane
dpppe	Bis(diphenylphosphino)pentane
equiv	Equivalent(s)
Et	Ethyl
<i>i</i> -Pr	Isopropyl
Mes	Mesityl
PL	Photoluminescence
py	Pyridyl
<i>t</i> -Bu	<i>Tert</i> -butyl
Tol	Tolyl

1 Introduction

During the last several decades, the chemistry of ligand-protected noble metal nanoparticles/clusters has progressed rapidly. Fundamental aspects have been addressed and practical uses have been found in diverse research areas including medicine, electronics, and catalysis [1–6]. The most prominent property of conventional gold particles (diameter >2 nm) is localized surface plasmon bands, which have been widely exploited for biomedical applications [4, 7]. On the other hand, for very small clusters in the subnanometer size regime ($d \sim 1$ nm or less), such plasmon resonances disappear and discrete electronic transitions emerge which are characteristic molecular properties [8–12]. Thus, it is now well recognized that the subnano-sized clusters are virtually different from conventional colloidal particles/clusters in terms of electronic structures and properties [8]. Especially in recent years, much attention has been paid to their unique optical properties since the discovery of photoluminescence of some ultrasmall gold clusters in this size regime [13]. The reactivity and catalysis of the ultrasmall metal entities have also attracted great interest [5].

Structurally defined molecular metal clusters offer nice models to establish the structure–property relationship in the subnanometer regime. Molecular structures of numerous phosphine- and thiolate-ligated gold clusters, which form major families in cluster chemistry, have been determined. From a structural standpoint, thiolate-capped clusters, whose molecular structures were extensively elucidated just recently, are interesting but somewhat complicated because the metal cores are covered by multiple gold-thiolate staples [14–18]. On the other hand, phosphine-capped gold clusters (PGCs) have simple core-shell structures composed of the inorganic moiety (metal core) and surrounding organic ligands (shell) because of the neutral character of phosphine, thus they provide a useful platform to assess the nature of the inner gold core moieties and organic–inorganic interfaces. Further, PGCs have a long history of studies to provide a large structure library. Surveying of the Cambridge Structural Database (CSD) (2012) has identified approximately 300 crystal structures of gold-based cluster compounds.

The first example of PGC can be traced back to the pioneering work by Malatesta in 1966 [19], but the structure could not be accurately defined. Later, in 1970s and early 1980s, definitive X-ray structure determinations were achieved independently mainly by a Nijmegen group [20–33] and Mingos et al. [34–43] for various PGCs with nuclearity of 5–13 [44–49]. Most of these clusters exploited monodentate phosphines as the ligands, revealing the general trend of the geometrical preference in the formation of ultrasmall clusters under unconstrained conditions. Through these studies, fundamental structure and bonding of this class of compounds were comprehensively established and were also interpreted theoretically [50–52]. Thereafter, major interests in ligand-coordinated gold clusters moved to heterometallic, higher-nuclearity (e.g., Au₃₉, Au₅₅), and thiolate-capped families. However, the interests in ultrasmall molecular PGCs have recently revisited [8, 53–55] in relation to the advances of structural chemistry of thiolate-capped clusters. Further, the use of state-of-the-art analytical instruments together with the advanced computation technology has opened the door to unusual cluster species.

Asides from conventional clusters, there is another line of studies on “Au(I)” clusters which do not contain formally zero-valent gold atoms [56, 57]. Further, there are extensive studies on clusters whose skeletons are constituted primarily by gold but contain other metal elements [58, 59] or encapsulated main group element (e.g., C, N) [60]. This chapter does not cover them and focuses on homoleptic and heteroleptic phosphine-coordinated pure-gold cluster compounds with formally mixed-valence character (formal averaged oxidation number lies between 0 and 1). Thus the general formula can be described as [Au_N(PR₃)_mX_s]^{z+} (*N* > *z*), in which tertiary phosphines (PR₃) serve as primary protecting ligands and additional ligands (X), such as halide and thiolate anions, sometimes coordinate with the surface metals as sub-ligands. This chapter first discusses the characterization and synthetic techniques of PGCs and then surveys the structural features and electronic absorptions/photoluminescence properties. Since the studies before 1990 established by the first generation have been already comprehensively summarized in literatures [25, 34, 35] and also in this book, emphases are placed on the recent advances in the clusters with unusual structures. In the last part of this chapter, the application of PGCs for stimuli-responsive chromic modules is also presented.

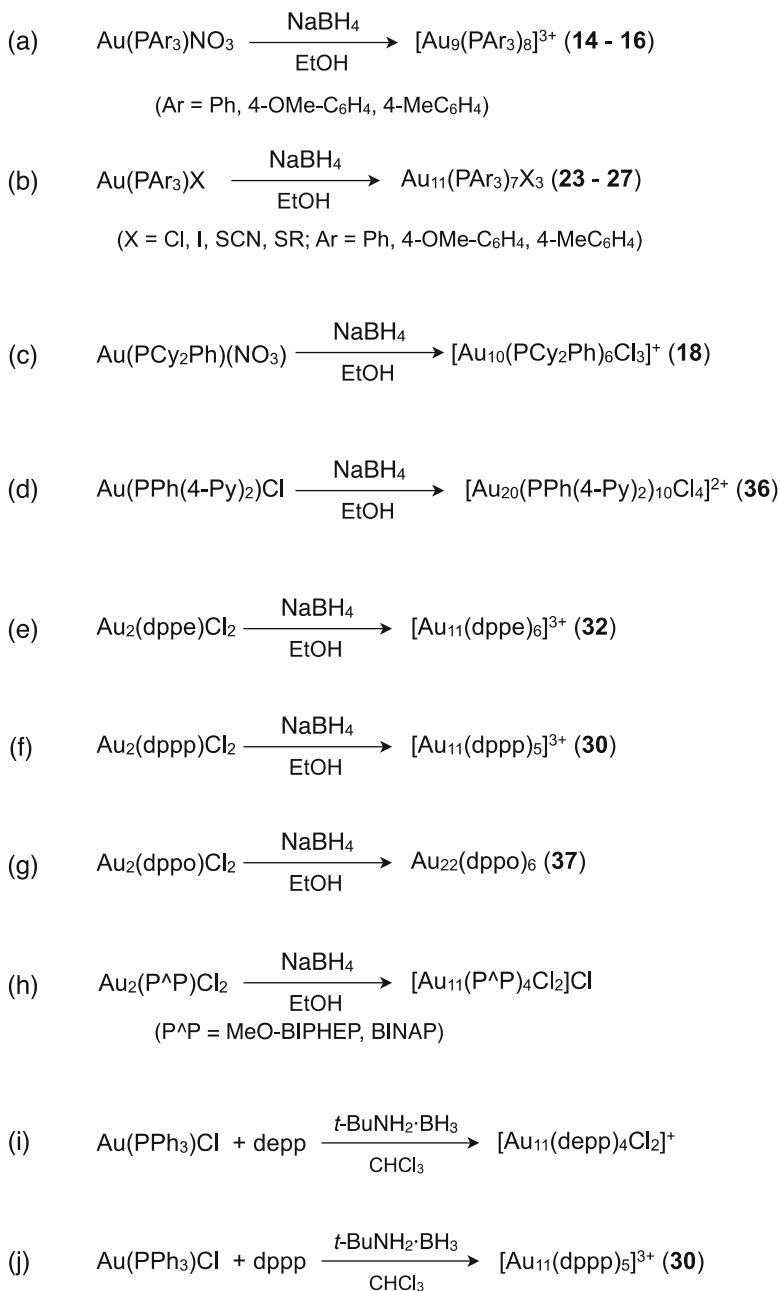
2 Characterization

Identification and characterization of PGCs have been achieved in terms of nuclearity (size), molecular formulae, and geometrical structures by various analytical techniques. Among them, single-crystal X-ray crystallography is still the most definitive technique to elucidate the geometrical structures, but it is limited to the clusters that give high-quality crystals suitable for the structure determination. Recently mass spectrometry coupled with soft-ionization techniques (e.g., electrospray ionization (ESI), matrix-assisted laser desorption ionization (MALDI)) are found to be powerful tools to obtain direct information about the molecular mass and formulae of cluster species. ESI-mass spectroscopy is especially useful since it can analyze solution samples, allowing the direct analyses of the reaction mixtures. However, one must note that the observed peak, especially before the purification procedure, may be a result of fragmentation/recombination in the gas phase, and the results sometimes strongly depend on the measurement conditions (e.g., voltage). Further, mass spectra give only molecular formula information so the geometrical structures must be deduced with the aid of other characterization methods. ^1H and ^{31}P NMR spectra are useful to investigate the dynamics of the coordinated ligands on the cluster surface, but are not suitable to obtain definitive molecular structures. TEM has been used to estimate the size and nuclearity of large clusters but the application for small clusters is limited because of the resolution limitation.

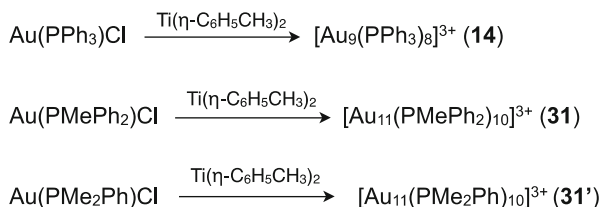
Electronic absorption (UV–visible) spectroscopy is classical but has been most conveniently utilized as a characterization tool. The spectral features of cluster species in the subnanometer-regime are unique to individual clusters and are sensitive to the structures/nuclearity of the cluster compounds, so it is possible to identify unknown species based on the spectral pattern of structurally identified authentic samples. Further, since the spectral profiles are closely correlated with the electronic structures, they are useful to understand the geometry- or nuclearity (size)-dependent profiles of PGCs. This aspect will be discussed in Sect. 5.

3 Synthesis

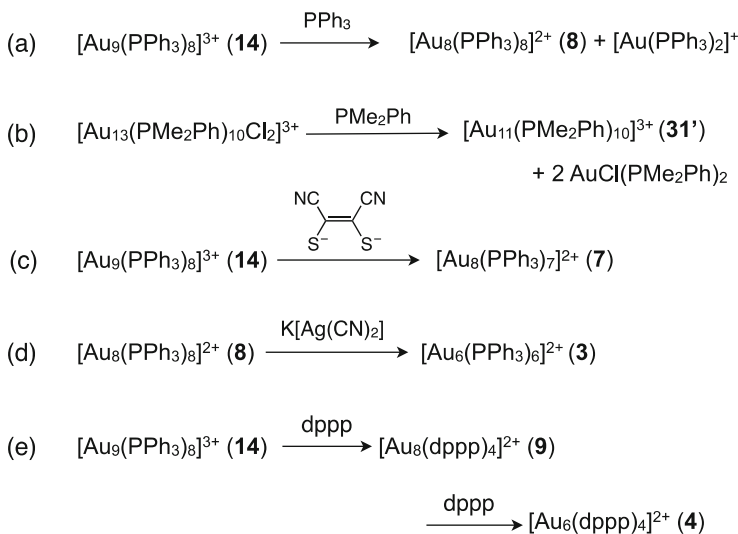
Generally, PGCs are synthesized in homogeneous solution either by the reduction of ionic gold sources (e.g., gold(I) phosphine complex, tetrachloroaurate) or by the post-synthetic methods involving the growth and/or etching of preformed PGCs. Other methods have also been known, but most of the synthetic procedures reported to date fall into these two categories. The representative examples were summarized in Schemes 1, 2, 3, 4, 5, 6, 7, 8, and 9 in terms of the reaction types.



Scheme 1 Selected examples of PGC syntheses via hydride reduction of gold(I) phosphine complexes



Scheme 2 Syntheses of Au₉ and Au₁₁ clusters by the reduction with zero-valent titanium reagent

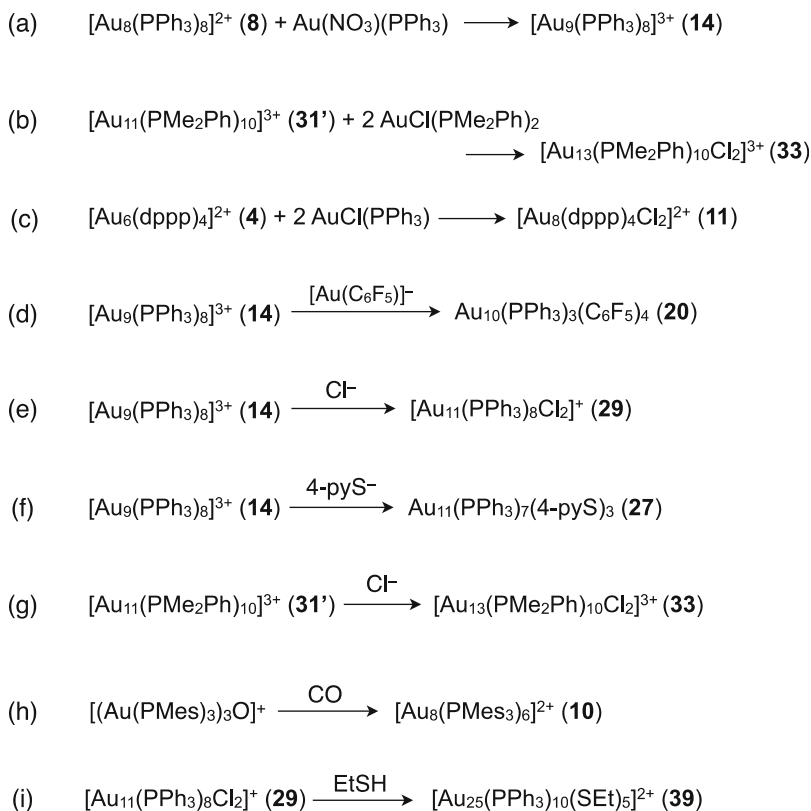
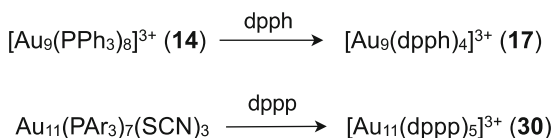
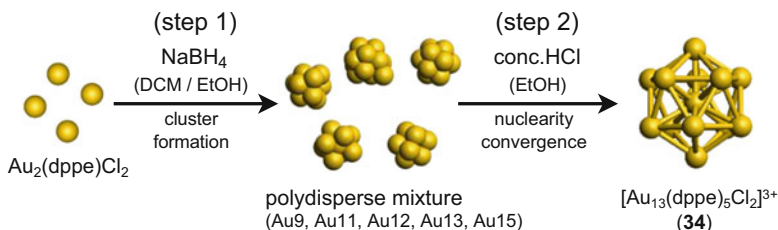


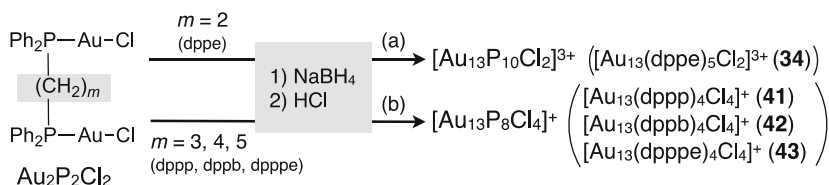
Scheme 3 Examples of PGC syntheses via etching reactions

3.1 Direct Syntheses from Gold Complex Ion or Bulk Gold

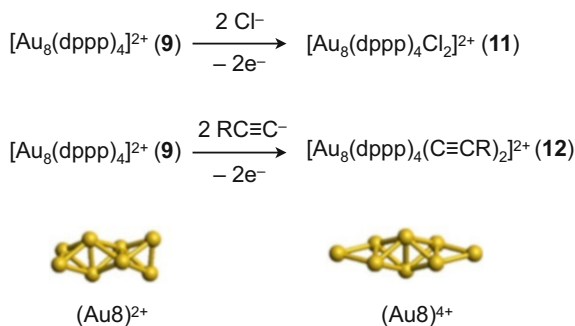
3.1.1 Borohydride or Borane Reduction of Gold(I) Phosphine Complex

The borohydride reduction of monophosphine gold(I) complex (Au(PR₃)X) in ethanol is the original recipe and has been most widely used as a conventional method, which generally yields Au₉ [27, 37, 38, 61, 62] or Au₁₁ species [19, 44–48, 63–65]. NaBH₄ is commonly exploited as the reducing agent, because of the ease in handling. From gold(I) triarylphosphine complex (Au(PAr₃)₃X) with a strongly coordinating anion (X=Cl, I, SCN, S-4-py), neutral deca-coordinated undecagold clusters Au₁₁(PAr₃)₇X₃ (e.g., **23–27**, Table 1) are preferentially formed (Scheme 1a), whereas the formation of cationic octa-coordinated nonagold cluster [Au₉(PAr₃)₈]³⁺ (e.g., **14–16**) is preferred when X is NO₃ with a weak coordinating character (Scheme 1a). The steric hindrance and the presence of additional coordination sites in the phosphine ligand affect the extent of the cluster growth processes.

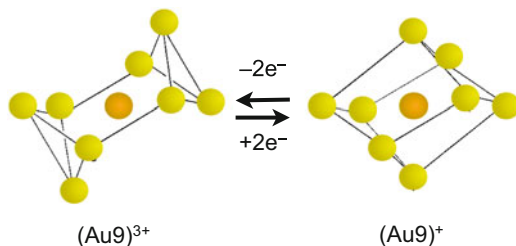
**Scheme 4** Examples of PGC syntheses via growth (aggregation) reactions**Scheme 5** Examples of simple ligand-exchange reaction**Scheme 6** Two-step synthesis of icosahedral Au_{13} cluster via HCl-promoted growth/etching



Scheme 7 Formation of two types of Au_{13} clusters



Scheme 8 Nucleophilic addition to $[\text{Au}_8(\text{dppp})_4]^{2+}$ (9) accompanying the oxidative skeletal isomerization

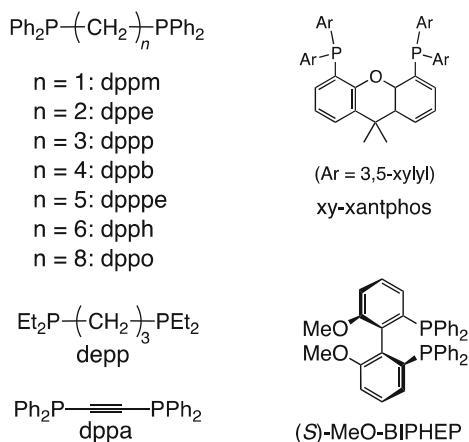


Scheme 9 Schematic illustration of the two-electron redox processes between $[\text{Au}_9(\text{PPh}_3)_8]^{3+}$ (14) and $[\text{Au}_9(\text{PPh}_3)_8]^+$

Reaction of $\text{Au}(\text{PCy}_2\text{Ph})(\text{NO}_3)$ with NaBH_4 affords $[\text{Au}_{10}(\text{PCy}_2\text{Ph})_6\text{Cl}_3]^+$ (18) (c) [39]. Recently, Wang et al. reported that the reduction of $\text{AuCl}(\text{PPh}(4\text{-py})_2)$ with NaBH_4 yields a larger cluster with an ionic formula $[\text{Au}_{20}(\text{PPh}(4\text{-py})_2)_{10}\text{Cl}_4]^{2+}$ (36), in which the pyridyl groups (py) additionally coordinate with the surface gold atoms (d) [66]. Diborane can be also utilized as the reducing agent. Reduction of $\text{Au}(\text{PPh}_3)\text{Cl}$ in benzene gives $\text{Au}_{55}(\text{PPh}_3)_{12}\text{Cl}_6$ [67], but its single-crystal structure is not available yet.

Diphosphines (P^\wedgeP) have also been used as the ligands in the borohydride reduction of chlorogold(I) complex ions (Scheme 1e–j). Similarly to the reduction of monophosphine complex, this reaction system generally affords deca-

coordinated $\text{Au}_{11}\text{L}_{10}$ -type (L =phosphine or Cl) clusters predominantly, but the ligand ratio ($\text{P}:\text{Cl}$) is different. For example, in the reduction of $\text{Au}(\text{PPh}_3)\text{Cl}$ with $t\text{-BuNH}_2\cdot\text{BH}_3$ in chloroform in the presence of C3-bridged diphosphine (dppp), the predominant formation of $\text{Au}_{11}\text{P}_{10}$ -type cluster ($[\text{Au}_{11}(\text{dppp})_5]^{3+}$, **30**) is detected in the mass spectra (j) [68]. We have also found that the simple NaBH_4 reduction of $\text{Au}_2(\text{dppp})\text{Cl}_2$ in ethanol gives **30** as the main cluster product (f) [69]. On the other hand, the mass spectrometric analyses of the reduction system $\text{Au}(\text{PPh}_3)\text{Cl}/t\text{-BuNH}_2\cdot\text{BH}_3$ coupled with non-phenyl type C3-bridged diphosphine ligand ($\text{Et}_2\text{P}(\text{CH}_2)_3\text{PEt}_2$, depp) showed the preferential formation of $\text{Au}_{11}\text{P}_8\text{Cl}_2$ -type cluster $[\text{Au}_{11}(\text{depp})_4\text{Cl}_2]^+$ (i) together with $[\text{Au}_{12}(\text{depp})_4\text{Cl}_3]^+$ and $[\text{Au}_{13}(\text{depp})_4\text{Cl}_3]^+$ [70]. Such $\text{Au}_{11}\text{P}_8\text{Cl}_2$ -type clusters are also obtained as the main cluster products in the NaBH_4 reduction of dinuclear chlorogold complexes of chiral diphosphines BINAP [71] and MeO-BIPHEP [72] in ethanol (h), which are identified by mass and absorption spectra but their single-crystal X-ray structures are not available.



On the other hand, the use of particular diphosphines results in the formation of different cluster species due to the steric and chelating effects of diphosphines. For example, the above $\text{Au}(\text{PPh}_3)\text{Cl}/t\text{BuNH}_2\cdot\text{BH}_3$ system coupled with C5- (dpppe, $\text{Ph}_2\text{P}(\text{CH}_2)_5\text{PPh}_2$) or C6-bridged (dpph, $\text{Ph}_2\text{P}(\text{CH}_2)_6\text{PPh}_2$) diphosphine gives $[\text{Au}_8(\text{P}^\wedge\text{P})_4]^{2+}$ and $[\text{Au}_{10}(\text{P}^\wedge\text{P})_4]^{2+}$ as the main cluster products. Wang et al. have recently reported that the NaBH_4 reduction of chlorogold(I) complex of C8-bridged diphosphine (dppo) affords a larger cluster $\text{Au}_{22}(\text{dppo})_6$ (**37**, Scheme 1g) [73]. We have also shown that the use of C2-bridged diphosphine (dppp) for the NaBH_4 reduction of chlorogold(I) complex in ethanol results in the formation of an Au_{11} species, which however accommodate a different number of coordinating phosphine ligands ($\text{Au}_{11}\text{L}_{12}$ type) (e) [74]. The ionic formula is $[\text{Au}_{11}(\text{dppe})_6]^{3+}$ (**32**), which exhibits an unusual green color. In this reaction, the cluster products are strictly dependent on the reaction medium. When the same reaction is conducted in CH_2Cl_2 / EtOH (50/50 v/v), the ESI-mass spectrum gives multiple signals

assignable to $[\text{Au}_9(\text{dppe})_5]^{3+}$, $[\text{Au}_{11}(\text{dppe})_5]^{3+}$, $[\text{Au}_{12}(\text{dppe})_5\text{Cl}]^{3+}$, $[\text{Au}_{13}(\text{dppe})_5\text{Cl}_2]^{3+}$, and $[\text{Au}_{15}(\text{dppe})_6\text{ClH}]^{3+}$ (Scheme 6, *vide infra*) [75]. On the other hand, the same reduction system from the C3-bridged complex $(\text{Au}_2(\text{dppp})_2\text{Cl}_2)$ in $\text{CH}_2\text{Cl}_2/\text{EtOH}$ (50/50 v/v) affords ESI-mass signals assignable to higher nuclearity clusters $[\text{Au}_{38}(\text{dppp})_9\text{Cl}_2]^{4+}$ and $[\text{Au}_{39}(\text{dppp})\text{Cl}_3]^{4+}$ [76]. These results imply that the cluster growth processes are not only governed by the intrinsic stability of the gold core but also notably affected by the steric and cheating effects of multidentate ligands and reaction conditions.

3.1.2 Other Methods

Other reducing agents have also been utilized. The utilization of $\text{Ti}(\eta\text{-C}_6\text{H}_5\text{CH}_3)_2$ developed by Mingos et al. affords $[\text{Au}_9(\text{PAr}_3)_8]^{3+}$ (**14**, **16**) from $\text{AuCl}(\text{PPh}_3)$ (Scheme 2) [36]. The same reduction system from $\text{Au}(\text{PMe}_2\text{Ph})\text{Cl}$ and $\text{Au}(\text{PMePh}_2)\text{Cl}$ results in the formation of deca-phosphine-coordinated Au_{11} cluster compounds having no Cl ligands on the cluster surface ($[\text{Au}_{11}(\text{PMePh}_2)_{10}]^{3+}$ (**31**) and $[\text{Au}_{11}(\text{PMe}_2\text{Ph})_{10}]^{3+}$ (**31'**) [34, 42]. Recently, $[\text{Au}_6(\text{xy-xantphos})_3]\text{Cl}$ (**5-Cl**) was isolated by recrystallization from the reaction mixture of $\text{Au}(\text{xy-xantphos})\text{Cl}$ and PhMe_2SiH [77].

HAuCl_4 instead of gold phosphine complex is usable as the starting gold source. Upon reduction of HAuCl_4 by NaBH_4 in the presence of trioctylphosphine in aqueous THF, $[\text{Au}_{13}(\text{POct}_3)_8\text{Cl}_4]^+$ is obtained as a minor product [76]. $[\text{Au}_{39}(\text{PPh}_3)_{14}\text{Cl}_6]\text{Cl}_2$ (**40-Cl**), which is, to date, the largest PGC characterized by single-crystal X-ray diffraction, was synthesized by the reduction of HAuCl_4 by NaBH_4 [78]. Recently, $[\text{Au}_{24}(\text{PPh}_3)_{10}(\text{SC}_2\text{H}_4\text{Ph})_5\text{X}_2]^+$ (**38**) was synthesized by Jin et al. through the NaBH_4 reduction of HAuCl_4 based on the Brust's two-phase method [79].

Several other gold sources have also been utilized. $[\text{Au}_7(\text{PPh}_3)_7]^+$ (**6**) can be prepared by the reaction of gold vapor with PPh_3 in toluene [31]. Azido complex $\text{AuN}_3(\text{PPh}_3)$ is also usable as a precursor, which affords $[\text{Au}_8(\text{PPh}_3)_8]^{2+}$ (**8**) upon photolysis in THF [80].

3.2 Post Synthesis

As noted in Sect. 3.1, Au_9 and Au_{11} clusters are frequently found as the primary products in the direct PGC synthesis from gold(I) precursors and thus appear to be relatively stable compounds. However, due to the flexible nature of the cluster skeletons and lability of Au–Au interactions, they can be easily converted into different cluster species via post-synthetic aggregation-mediated growth and degradation-mediated etching processes, thus acting as useful intermediates for a variety of PGC compounds.

3.2.1 Etching Reactions

Several etching (degradation) reactions of monophosphine-protected Au₉ and Au₁₁ clusters upon treatment with free phosphines have been reported. [Au₈(PPh₃)₈]²⁺ (**8**) can be obtained by the reaction of [Au₉(PPh₃)₈]³⁺ (**14**) with free PPh₃, which accompanies the liberation of Au(PPh₃)⁺ (Scheme 3a) [20, 49]. In a similar fashion, [Au₁₁(PMe₂Ph)]³⁺ (**31'**) can be synthesized from [Au₁₃(PMe₂Ph)₁₀Cl₂]³⁺ (**33**) in the presence of free PMe₂Ph (b) [34]. Reaction of [Au₉(PPh₃)₈]³⁺ (**14**) with sodium maleonitriledithiolate (MNTNa₂:Na₂S₂C₂(CN)₂) affords hepta-coordinated Au₈ cluster ([Au₈(PPh₃)₇]²⁺, **7**) (c) [41], which can also be obtained by the phosphine abstract reaction of **8** by [RhCl(cyclooctene)₂]₂ [30]. The reaction of [Au₈(PPhR₂)₈](NO₃)₂ (R=Ph, **8**-NO₃) in the presence of K[Ag(CN)₂] affords edge-sharing bitetrahedral [Au₆(PPhR₂)₈]²⁺ (R=Ph (**3**), 2-MeC₆H₄, Cy) (d) [40].

The etching reactions during the ligand exchange reaction with diphosphine have also been reported. The treatment of [Au₉(PPh₃)₈](NO₃)₃ (**14**-NO₃) with excess free dppp results in the formation of core+*exo* type [Au₆(dppp)₄]²⁺ (**4**) (e) [26]. As an intermediate cluster species in this reaction, [Au₈(dppp)₄]²⁺ (**9**) have been isolated and identified by mass spectrometry and single-crystal X-ray diffraction studies [81].

3.2.2 Growth Reactions

The addition reaction of mononuclear gold species to preformed cluster species results in the growth of the cluster nuclearity. The reaction of [Au₈(PPh₃)₈]²⁺ (**8**) with Au(NO₃)(PPh₃) leads to the formation of [Au₉(PPh₃)₈](NO₃)₃ (**14**-NO₃) (Scheme 4a) [21, 31]. Likewise, [Au₁₁(PMe₂Ph)₁₀]³⁺ (**31'**) grows to [Au₁₃Cl₂(PMe₂Ph)₁₀]³⁺ (**33**) by the addition of AuCl(PMe₂Ph) (b) [34]. The treatment of Au₆(dppp)(NO₃)₂ (**4**-NO₃) with Au(PPh₃)Cl results in the formation of [Au₈(dppp)Cl₂]²⁺ (**11**) (c) [81]. An organometallic cluster Au₁₀(PPh₃)₃(C₆F₅)₄ (**20**) can be obtained by the reaction of [Au₉(PPh₃)₈]³⁺ (**14**) with (NBu₄)[Au(C₆F₅)] (d) [82].

The reactions with nucleophilic agents are known to induce aggregation reactions between several cluster molecules. This reaction is unpredictable, but sometimes useful for the syntheses of higher nuclearity clusters. In the presence of Cl⁻ with coordinating capability, [Au₁₁(PMe₂Ph)₁₀]³⁺ and [Au₉(PPh₃)₈]³⁺ (**14**) are converted into [Au₁₃Cl₂(PMe₂Ph)₁₀]³⁺ (**33**) [36] and [Au₁₁(PPh₃)₈Cl₂]⁺ (**29**) [21, 83], respectively (Scheme 4e and g). The reaction of [Au₉(PPh₃)₈]³⁺ (**14**) with 4-pyridinethiol in alkaline methanol results in the formation of Au₁₁(PPh₃)₇(4-pyS)₃ (f) [84]. Shichibu et al. reported the synthesis of [Au₂₅(PPh₃)₁₀(SEt)₅Cl₂]²⁺ (**39**) by the reaction of [Au₁₁(PPh₃)₈Cl₂]Cl (**29**-Cl) and ethanethiol [85].

For other examples, the reduction of trinuclear oxonium salt [Au(PMe)₃]₃O]⁺ by CO affords hexa-coordinated Au₈ cluster [Au₈(PMe)₃]₆]²⁺ (**10**) (Scheme 4h) [86]. The decomposition of trinuclear hydrazido complex [(AuPPh₃)₃NNR₂]BF₄ leads to

the formation of $[\text{Au}_6(\text{PPh}_3)_6]^{2+}$ (**3**) [87], which is isostructural to that obtained by the silver-mediated etching reaction of $[\text{Au}_8(\text{PPh}_3)_8]^{2+}$ (**8**).

3.2.3 Ligand Exchange Reactions

As noted above, the reaction of once generated clusters with free ligands often results in the nuclearity alteration through the etching and growth of the cluster cores, but simple exchange reactions with the retention of the cluster nuclearity and structure take place when appropriate free ligands are utilized. For example, $[\text{Au}_{11}(\text{dppp})_5]^{3+}$ (**30**) is obtained by the reaction of $[\text{Au}_{11}(\text{P}(4\text{-ClC}_6\text{H}_4)_3)_7(\text{SCN})_3]^{3+}$ with dppp (Scheme 5) [24]. Likewise, the reaction of dppe with $[\text{Au}_9(\text{PPh}_3)_8](\text{NO}_3)_3$ (**14-NO}_3**) with four equiv of dppe affords $[\text{Au}_9(\text{dppe})_4]^{3+}$ (**17**) quantitatively [88].

3.2.4 Growth/Etching During Crystallization Process

Due to the soft potential surface of gold clusters, crystallization process sometimes allows the formation of unexpected cluster species that is different from the original cluster in the mother liquors. For example, crystallization of $[\text{Au}_8(\text{PPh}_3)_7][\text{S}_2\text{C}_2(\text{CN})_2]$ from $\text{CH}_2\text{Cl}_2/\text{MeCN}$ results in the formation of the crystals of $\text{Au}_{10}(\text{PCy}_3)_7(\text{MNT})$ (**19**) [41]. The formation of crystals containing Au_7 and Au_9 clusters has been reported when the polyoxometalate and fullerene salts of $[\text{Au}_8(\text{PPh}_3)_8]^{2+}$ are crystallized [61, 89]. Very recently, crystals of $\text{Au}_{14}(\text{PPh}_3)_8(\text{NO}_3)_4$ (**35**) have been isolated during the crystallization process in the $\text{Au}_9(\text{PPh}_3)_8(\text{NO}_3)_3$ (**14-NO}_3**) synthesis by the $\text{Au}(\text{PPh}_3)\text{NO}_3/\text{NaBH}_4$ system [90].

3.2.5 Nuclearity Convergence Through Simultaneous Etching/Growth

We have recently found that HCl has a unique capability to promote the etching and growth of PGCs [75, 76]. Through the simultaneous etching/growth processes, a polydisperse mixture of several dppe-coordinated clusters, which was formed by the NaBH_4 reduction of $\text{Au}_2(\text{dppe})\text{Cl}_2$ in $\text{CH}_2\text{Cl}_2/\text{EtOH}$, is exclusively converted into $[\text{Au}_{13}\text{Cl}_2(\text{dppe})_5]^{3+}$ (**34**) upon treatment with aqueous HCl (12 M) in EtOH (Scheme 6). This method is practically useful, allowing gram-scale preparation of icosahedral Au_{13} cluster (total yield exceeds 70%). Other protonic acids such as acetic acid and sulfuric acid, and tetraethyl ammonium chloride also served as promoters but are much inferior to hydrochloric acid, indicating that the effective nuclearity convergence is a result of growth/etching under thermodynamic conditions by the cooperation of acidic proton and chloride anion. The chelation effect of the diphosphine ligands plays a critical role in keeping the cluster structure and also affects the composition of the coordinating ligands of the final cluster products. With monophosphine ligand, the intermediate cluster species does not survive

the strongly acidic condition, while the use of diphosphine ligands with a longer alkyl bridge (dppp, dppb, dpppe) results in the preferential formation of $[\text{Au}_{13}\text{Cl}_4(\text{P}^{\wedge}\text{P})_4]^{3+}$ (**41–43**) (Scheme 7).

3.2.6 Redox Reactions

As mentioned in the above paragraphs, the addition of nucleophiles such as Cl[−] to monophosphine-coordinated clusters promotes the aggregation-induced growth of the cluster core. However, we recently found that the nucleophilic reaction towards $[\text{Au}_8(\text{dppp})_4]^{2+}$ (**9**) proceeds with the retention of the nuclearity but accompanies two-electron autoxidation and rearrangement of the cluster skeleton[91]. For instance, the reactions with nucleophiles such as halide and acetylide anions afford $[\text{Au}_8(\text{dppp})_4\text{X}_2]^{2+}$ ($\text{X}=\text{Cl}$ (**11**), $\text{X}=\text{C}\equiv\text{CPh}$ (**12**)), where the charge of the Au_8 skeleton is altered from 2+ to 4+ (Scheme 8). In this relation, electrochemical two-electron redox processes between $[\text{Au}_9(\text{PPh}_3)_8]^{3+}$ (**14**) and $[\text{Au}_9(\text{PPh}_3)_8]^+$, which accompany the skeletal rearrangement from toroidal to spherical, have also been reported (Scheme 9) [32, 92]. The large structural change may reflect the soft potential energy surface of this class of compounds.

3.2.7 Summary

A variety of PGCs can be synthesized in good yields when the appropriate reagents and pathways are used. However the cluster products are generally unpredictable and vary significantly with the subtle difference of synthetic parameters (methods, conditions, reagents, and so on).

4 Geometrical Structure

As noted in Sect. 2, single-crystal X-ray crystallography is the sole definitive method to elucidate the 3-dimensional structural features. PGCs with a nuclearity of 5, 6, 7, 8, 9, 10, 11, 13, 14, 20, 22, 24, 25, and 39 have been structurally identified. For selected examples, geometrical descriptions and Au–Au bond distances are summarized in the nuclearity order (Tables 1 and 2). Centered polyhedral geometries are generally favored because the center-to-peripheral interactions effectively enhance the stability of cluster skeleton. The majority of the clusters with $N \geq 8$ fall into this category. However, the use of sterically hindered ligands or chelating diphosphines sometimes allows the generation of exceptional structures that cannot be described only with polyhedra.

Table 1 Geometrical structures of crystallographically defined PGCs with nuclearity (N) of 5–13

	Counter anion	Geometry	Au–Au dist. (Å)	References
$(N = 5)$				
$[\text{Au}_5(\text{dppm})_3(\text{Ph}_2\text{PCHPhPh}_2)]^{2+}$ (1)	NO_3	Tetrahedron + 1 <i>exo</i>	2.702–3.013	[48]
$(N = 6)$				
$[\text{Au}_6(\text{PPh}_2\text{C}_6\text{H}_4)_4]^{2+}$ (2)	SbF_6	Octahedron	2.721–3.155	[93]
$[\text{Au}_6(\text{PPh}_3)_6]^{2+}$ (3)	NO_3	Edge-sharing bitetrahedron	2.652–2.839	[40]
$[\text{Au}_6(\text{dppp})_4]^{2+}$ (4)	NO_3	Tetrahedron + 2 <i>exo</i>	2.630–2.923	[26]
$[\text{Au}_6(\text{xy-xanphos})_3]^{1+}$ (5)	Cl	Face-sharing tritetrahedron	2.653–3.104	[77]
$(N = 7)$				
$[\text{Au}_7(\text{PPh}_3)_7]^{+}$ (6)	OH	Pentagonal bipyramid	2.582–3.007	[31, 94]
	C_{60}	Pentagonal bipyramid	2.561–3.092	[89]
$(N = 8)$				
$[\text{Au}_8(\text{PPh}_3)_7]^{2+}$ (7)	NO_3	Capped centered chair ^a	2.629–2.942	[22]
$[\text{Au}_8(\text{PPh}_3)_8]^{2+}$ (8)	AZS	Capped centered chair ^a	2.689–2.938	[49]
	PF_6	Capped centered chair ^a	2.634–2.960	[20]
	$\text{SiMo}_{12}\text{O}_{40}$	Capped centered chair ^a	2.650–2.909	[95]
$[\text{Au}_8(\text{dppp})_4]^{2+}$ (9)	NO_3	Edge-sharing tritetrahedron	2.616–2.752	[81]
$[\text{Au}_8(\text{PMes}_3)_6]^{2+}$ (10)	BF_4	Tetrahedron + 4 <i>exo</i>	2.616–2.752	[86]
$[\text{Au}_8(\text{dppp})_4\text{Cl}_2]^{2+}$ (11)	PF_6	Edge-sharing bitetrahedron + 2 <i>exo</i>	2.607–2.896	[81]
$[\text{Au}_8(\text{dppp})_4(\text{C}\equiv\text{CPh})_2]^{2+}$ (12)	NO_3	Edge-sharing bitetrahedron + 2 <i>exo</i>	2.648–3.072	[91]
$[\text{Au}_8(\text{dppa})_4\text{Cl}_2]^{2+}$ (13)	ClO_4	Edge-sharing bitetrahedron + 2 <i>exo</i>	2.619–3.052	[96]
$(N = 9)$				
$[\text{Au}_9(\text{PPh}_3)_8]^{3+}$ (14a)	NO_3	Bicapped centered chair (butterfly) ^a	2.675–2.880	[62]
$[\text{Au}_9(\text{PPh}_3)_8]^{3+}$ (14b)	$\text{PW}_{12}\text{O}_{40}$	Bicapped centered chair (butterfly) ^a	2.688–2.926	[61]
	$\text{PW}_{12}\text{O}_{40}$	Centered crown	2.662–2.806	[61]
	$\text{PMo}_{12}\text{O}_{40}$	Centered crown	2.661–2.810	[95]
$[\text{Au}_9(\text{P}[\textit{p}\text{-Tol}]_3)_8]^{3+}$ (15)	PF_6	Bicapped centered chair (butterfly) ^a	2.686–2.891	[27]
$[\text{Au}_9(\text{P}[\textit{p}\text{-MeOC}_6\text{H}_4]_3)_8]^{3+}$ (16a)	BF_4	Centered crown	2.651–2.838	[37]
	NO_3	Centered crown	2.659–2.843	[38]

[Au ₉ (P(<i>p</i> -MeOC ₆ H ₄) ₃) ₈] ³⁺ (16b)	NO ₃	Bicapped centered chair (butterfly) ^a	2.689–2.899	[38]
[Au ₉ (dpph) ₄] ³⁺ (17)	PW ₁₂ O ₄₀	Centered crown	2.643–3.249	[88]
(<i>N</i> = 10)				
[Au ₁₀ (PPhC ₆ H ₄) ₃ Cl ₃] ⁺ (18)	NO ₃	Tricapped centered chair (toroidal) ^a	2.666–2.941	[39]
Au ₁₀ (PPh ₃) ₇ (MNT) ₂ (19)	–	Tricapped centered chair (toroidal) ^a	2.567–3.055	[41]
Au ₁₀ (PPh ₃) ₅ (C ₆ F ₅) ₄ (20)	–	Tricapped centered chair (toroidal) ^a	2.639–2.964	[82]
Au ₁₀ (PPh ₃) ₈ Cl(NCO) (21)	–	Capped centered square antiprism (spherical)	2.635–3.174	[97]
[Au ₁₀ (PPh ₃) ₈ Cl] ⁺ (22)	PF ₆	Capped centered square antiprism (spherical)	2.637–3.151	[98]
(<i>N</i> = 11)				
Au ₁₁ (PPh ₃) ₇ Cl ₃ (23)	–	Tetracapped centered chair ^a	2.608–2.968	[65]
Au ₁₁ (PPh ₃) ₇ I ₃ (24)	–	Tetracapped centered chair ^a	2.634–3.193	[45]
Au ₁₁ (P(<i>p</i> -FC ₆ H ₄) ₃) ₇ I ₃ (25)	–	Tetracapped centered chair ^a	2.670–3.184	[47]
Au ₁₁ (P(<i>m</i> -CF ₃ C ₆ H ₄) ₃) ₇ Cl ₃ (26)	–	Tetracapped centered chair ^a	2.663–3.126	[99]
Au ₁₁ (PPh ₃) ₇ (4-pyS) ₃ (27)	–	Tetracapped centered chair ^a	2.629–3.122	[84]
[Au ₁₁ (PPh ₃) ₇ (CNiPr) ₂] ²⁺ (28)	PF ₆	Tetracapped centered chair ^a	2.670–3.127	[33]
[Au ₁₁ (PPh ₃) ₈ Cl ₂] ⁺ (29)	W ₆ O ₁₉	Tetracapped centered chair ^a	2.625–3.185	[88]
[Au ₁₁ (dppp) ₅] ³⁺ (30)	SCN	Tetracapped centered chair ^a	2.669–3.088	[29]
[Au ₁₁ (PMePh ₂) ₁₀] ³⁺ (31)	C ₂ B ₉ H ₁₂	Capped centered square antiprism	2.646–3.048	[42]
[Au ₁₁ (dppe) ₆] ³⁺ (32)	SbF ₆	Butterfly Au ₉ + 2 <i>exo</i>	2.608–3.216	[74]
(<i>N</i> = 13)				
[Au ₁₃ (PMe ₂ Ph) ₁₀ Cl ₂] ³⁺ (33)	PF ₆	Icosahedron	2.715–2.955	[36]
[Au ₁₃ (dppe) ₅ Cl ₂] ³⁺ (34)	SbF ₆	Icosahedron	2.696–2.974	[75]

^aCan also be described as a derivative or substructure of icosahedral Au₁₃

4.1 Centered Polyhedral Clusters

4.1.1 $N \leq 13$

Crystal structures of PGCs with $8 \leq N \leq 13$ were extensively studied before 1990, and the general preference centered polyhedral geometries have been almost established. The majority of these centered clusters have skeletal structures based on centered icosahedron, which can also be described as capped centered hexagonal chairs. Such icosahedron-based structures are found for a series Au_8L_7 , Au_9L_8 , Au_{10}L_9 , and $\text{Au}_{11}\text{L}_{10}$ clusters, which finally complete with the icosahedral $\text{Au}_{13}\text{L}_{12}$ -type clusters (Table 1). Representative examples are shown in the structures of **7** (Au_8L_7), **8** (Au_8L_7), **18** (Au_{10}L_9), **23** ($\text{Au}_{11}\text{L}_{10}$), **30** ($\text{Au}_{11}\text{L}_{10}$), and **34** ($\text{Au}_{13}\text{L}_{12}$) (Fig. 1). The exceptional structures that cannot be described based on icosahedron are also found in several cases. For example, Mingos et al. reported green and golden-brown crystals of $[\text{Au}_9(\text{P}(4\text{-MeOC}_6\text{H}_4)_3)_8](\text{NO}_3)_3$ (**16-NO**₃) and showed that the former has a bicapped chair D_{2h} geometry derived from icosahedron whereas the latter has a centered crown geometry [38]. The interconversion between the two forms seems easy since they share a common structure in solution. The crown geometries have also been found in the several polyoxometalate salts of Au_9P_8 clusters. Jansen et al. recently reported that the appropriate choice of recrystallization solvents allows the selective formation of either of the two skeletal geometries of **14**· $\text{PW}_{12}\text{O}_{40}$ (Fig. 2) [61].

As other examples of deviation from icosahedron-derived structures, capped centered square antiprism (approximately D_{4d} symmetry) geometries have been reported for $[\text{Au}_{11}(\text{PMePh}_2)_{10}]^{3+}$ (**31**) (Fig. 1) [42], which is obviously different from the icosahedron-based structures with approximately C_{3v} symmetry found in the conventional $\text{Au}_{11}(\text{PAr}_3)_{10}$ clusters for various combinations of phosphine, sub-ligands, and counter anion [28, 29, 33, 47, 65, 84, 88, 99] (Table 1 and **23** and **30** in Fig. 1). This geometry can also be viewed as a capped crown, which is also found for Au_{10}L_9 clusters (**22** in Fig. 1) [98].

As mentioned in previous papers and reviews [35, 42], the center-to-peripheral radial bond distances are shorter than the peripheral bond distances, indicating the crucial contribution of radial bonding to the stability of cluster skeleton. The overall shape of these clusters can be categorized into toroidal (ellipsoidal, 2D) and hemispherical/spherical (3D), which have been accounted for in terms of polyhedral electron counting and molecular orbital calculations [34, 51].

4.1.2 Higher-Nuclearity Clusters

Several examples of higher-nuclearity centered clusters have appeared recently and their structures are shown in Fig. 3. Simon et al. showed that the crystal structure of $[\text{Au}_{14}(\text{PPh}_3)_8(\text{NO}_3)_4]$ (**35**) exhibits a unique geometry, in which two face-sharing tetrahedron dimers are connected by four AuNO_3 units [90]. The distance between

Table 2 Geometrical structures of higher nuclearity PGCs with $N > 13$

Cluster formula	Counter anion	Description	Au–Au dist. (Å)	References
$\text{Au}_{14}(\text{PPh}_3)_8(\text{NO}_3)_4$ (35)	–	Trigonal bipyramid dimer linked by 4 AuNO_3	2.582–2.984	[90]
$[\text{Au}_{20}(\text{PPh}\{4\text{-Py}\}_2)_{10}\text{Cl}_4]^{2+}$ (36)	Cl	Edge-sharing icosahedral Au_{11} dimer	2.644–3.189	[66]
$\text{Au}_{22}(\text{dppo})_6$ (37)	–	Icosahedral Au_{11} dimer	2.631–3.227	[73]
$[\text{Au}_{24}(\text{PPh}_3)_{10}(\text{SC}_2\text{H}_4\text{Ph})_5\text{X}_2]^+$ (38)	Unknown	Incomplete icosahedral Au_{12} dimer	2.721–2.990	[79]
$[\text{Au}_{25}(\text{PPh}_3)_{10}(\text{SEt})_5\text{Cl}_2]^{2+}$ (39)	SbF_6	Vertex-sharing icosahedral Au_{13} dimer	2.695–3.116	[85]
$[\text{Au}_{39}(\text{PPh}_3)_{14}\text{Cl}_6]^{2+}$ (40)	Cl	1:9:9:1:9:9:1 layered	2.690–3.112	[78]

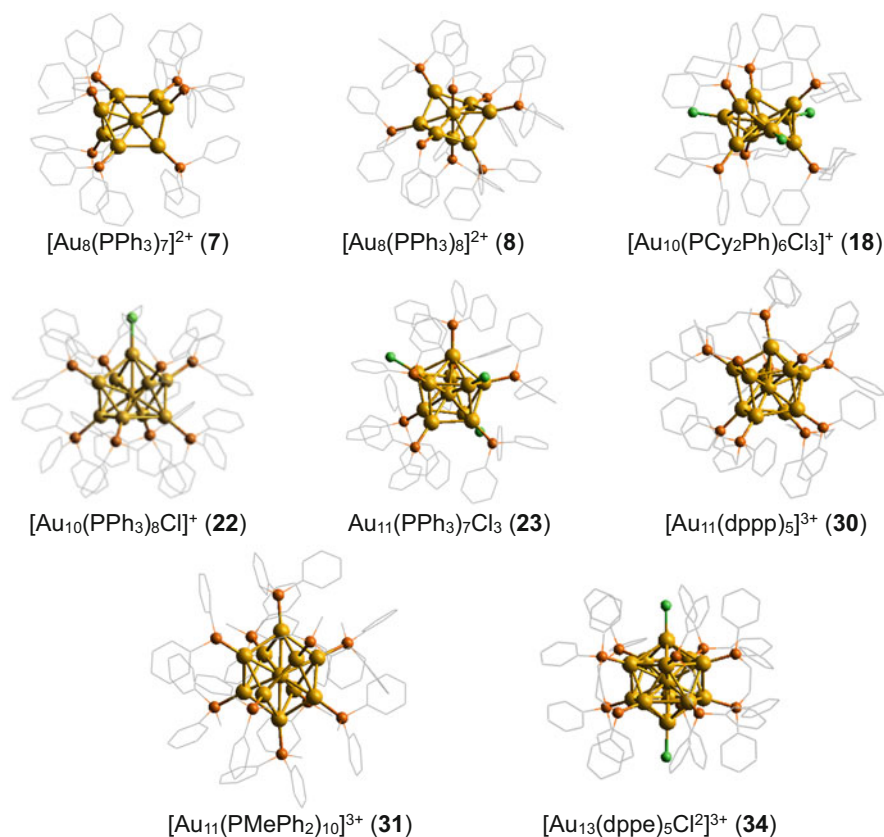


Fig. 1 Single-crystal X-ray structures of $[\text{Au}_8(\text{PPh}_3)_7]^{2+}$ (**7**), $[\text{Au}_8(\text{PPh}_3)_8]^{2+}$ (**8**), $[\text{Au}_{10}(\text{PPhCy}_2)_6\text{Cl}_3]^+$ (**18**), $[\text{Au}_{10}(\text{PPh}_3)_8\text{Cl}]^+$ (**22**), $\text{Au}_{11}(\text{PPh}_3)_7\text{Cl}_3$ (**23**), $[\text{Au}_{11}(\text{dppp})_5]^{3+}$ (**30**), $[\text{Au}_{11}(\text{PMePh}_2)_{10}]^{3+}$ (**31**) and $[\text{Au}_{13}(\text{dppe})_5\text{Cl}_2]^{3+}$ (**34**). For counter ions (see Table 1). For **7**, **8**, **18**, **23**, **30**, and **34**, the gold core units can be described as capped chairs (icosahedron derivatives), whereas those of **22** and **31** can be described as D_{4d} bicapped crowns

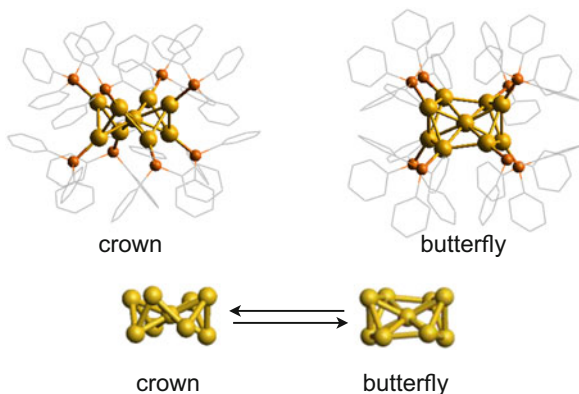


Fig. 2 Single-crystal X-ray structures of two isomeric structures of the cluster moieties of $[\text{Au}_9(\text{PPh}_3)_8](\text{PW}_{12}\text{O}_{40})$ (**14**· $\text{PW}_{12}\text{O}_{40}$)

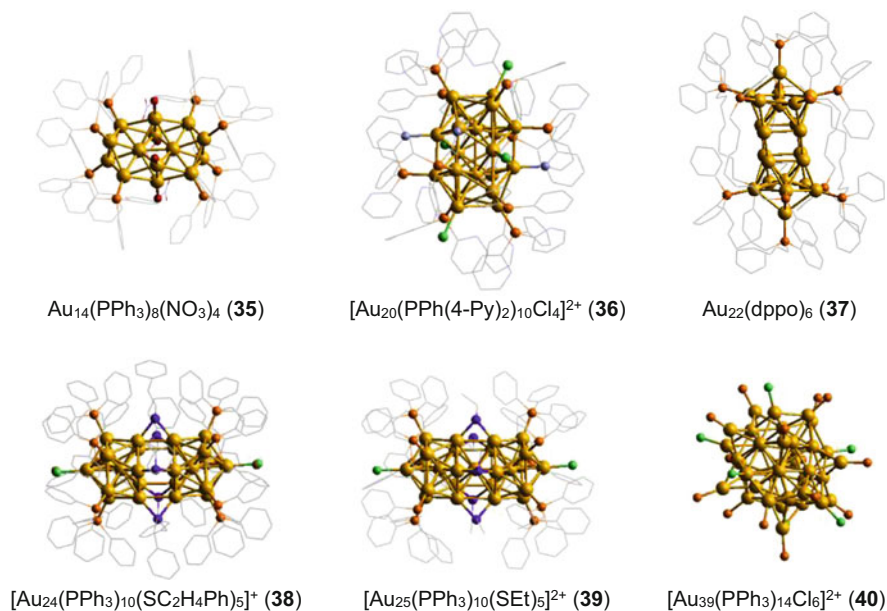


Fig. 3 Single-crystal X-ray structures of Au_{14} (**35**), Au_{20} (**36**), Au_{22} (**37**), Au_{24} (**38**), Au_{25} (**40**) and Au_{39} (**41**) clusters. Counter anion: Cl (**36**), SbF_6 (**40**), Cl (**41**)

two nearest neighbor nitrated gold atoms are very short (2.58 Å). The icosahedral Au_{13} and quasi-icosahedral Au_{11} can serve as the building units of prolate-shaped higher nuclearity clusters when additional attractive forces or steric effects are applied. Q. M. Wang et al. recently reported the structure of $[\text{Au}_{20}(\text{PPy}_2\text{Ph})_{10}\text{Cl}_4]^{2+}$ (**36**), which can be viewed as an edge-sharing dimer of icosahedron-based Au_{11} cluster [66]. The additional coordination of pyridyl groups to the cluster surface

appears to assist the holding of the cluster skeleton. Wang et al. reported that $\text{Au}_{22}(\text{dppo})_6$ (**37**), although its charge is ambiguous, has a structure composed of two quasi-icosahedral Au_{11} units fused via four short Au–Au bridges [73]. There are also examples of the utilization of thiolate as bridging ligands. Shichibu et al. demonstrated that the structure of $[\text{Au}_{25}(\text{PPh}_3)_{10}(\text{SC}_2\text{H}_5)\text{Cl}_2]^{2+}$ (**39**) cluster can be defined as two Au_{13} cluster units joined through five thiolate bridges by vertex sharing [85]. An analogous thiolate-bridged PGC composed of two incomplete icosahedral Au_{12} units, in which one vertex atom of Au_{13} icosahedron is missing, has been recently reported by Jin et al. for $[\text{Au}_{24}(\text{PPh}_3)_{10}(\text{SC}_2\text{H}_4\text{Ph})_5\text{X}_2]^+$ ($\text{X}=\text{Br}$ or Cl , **38**) [79]. The Au–Au bond distances in these icosahedron-based clusters (**36–39**) are similar to those of smaller centered clusters, being in the range 2.63–3.23 Å (Table 2). Short distances less than 2.7 Å are observed for the center-peripheral radial bonds.

On the other hand, the structures of $[\text{Au}_{39}(\text{PPh}_3)_{14}\text{Cl}_6]\text{Cl}_2$ **40·Cl** is exceptional, being defined as a 1:9:9:1:9:9:1 layered hcp/hcp', which is virtually different from the icosahedron-based structure.

4.2 Non-centered Polyhedral Clusters

Lower nuclearity clusters favor condensed polyhedra rather than centered geometries (Fig. 4). For hexanuclear clusters ($N = 6$), the simplest geometry is octahedron. Bellon et al. reported an octahedral structure for $[\text{Au}_6\{\text{P}(\text{p-Tol})_3\}_6]^{3+}$ [48], but later it is identified to be a carbon-centered octahedron [100]. Very recently Echavarren et al. reported organometallic Au_6 clusters protected by ortho-aurated PPh_3 ligands $[\text{Au}_6(\text{PPh}_2\text{C}_6\text{H}_4)_4](\text{SbF}_6)_2$ (**2·SbF₆**), though their gold atoms are formally monovalent, adopt an octahedron [93]. In this structure, the octahedron is severely distorted, where some edges are short in the range 2.72–2.75 Å but the other bonds are longer than 3.10 Å. Au_6 cluster can also adopt tetrahedron-based geometries. Mingos et al. reported an edge-sharing bitetrahedral structure of $[\text{Au}_6(\text{PPh}_3)_6]^{2+}$ (**3**) [40], where the shared (2.652 Å) and terminal (2.662 and 2.669 Å) edges are significantly shorter than the other eight edges (2.762–2.839 Å) (Table 3). We have recently shown that an edge-sharing Au_4 tetrahedron trimer ($[\text{Au}_8(\text{dppp})_4]^{2+}$, **9**), which is an extended version of **3**, has a similar structural feature [81]. The bond distances of two shared and terminal edges are 2.623 and 2.607 Å, respectively, which are again shorter than the distances of the remaining connecting bonds (2.824–2.896 Å) (Table 3). A face-sharing tritetrahedral structure has been reported for $[\text{Au}_6(\text{xy-xantphos})_3]\text{Cl}$ (**5**), where the edge shared by three Au_4 tetrahedra shows a short distance (2.653 Å) [77]. Thus, in the structures based on Au_4 tetrahedron, the short distances are found for the shared and terminal edges.

Fig. 4 Single-crystal X-ray structures of non-centered polyhedral Au₆, Au₇, and Au₈ clusters. Counter anion: NO₃ (**1**, **2**, **9**), Cl (**5**), C₆₀ (**6**)

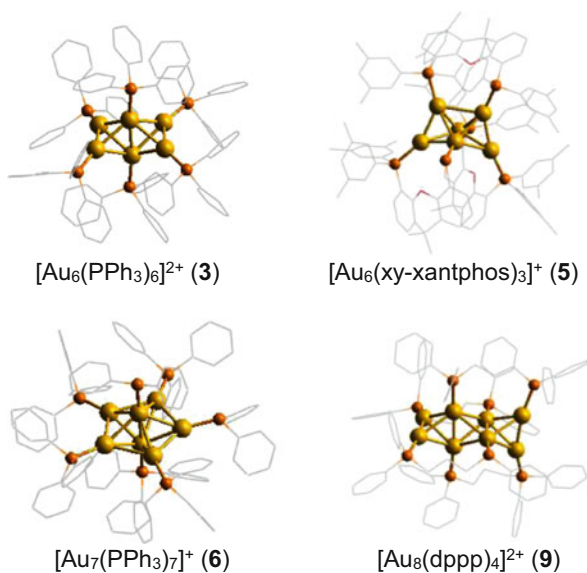


Table 3 Au–Au bond distances (Å) of Au₄ tetrahedron-based clusters

	Polyhedral core			<i>exo</i> -to-core	References
	Distance range (mean)	Shared edge	Terminal edge		
<i>Tetrahedral</i>					
[Au ₅ (dppm) ₃ (Ph ₂ PCHPPh ₂)](NO ₃) ₂ (1 ·NO ₃)	2.702–3.006 (2.828)			3.013	[23]
[Au ₆ (dppp) ₄](NO ₃) ₂ (4 ·NO ₃)	2.630–2.923 (2.825)	–	2.630 ^a	2.798	[26]
[Au ₈ (PMes ₃) ₆](BF ₄) ₂ (10 BF ₄)	2.697–2.711 (2.707)	–	–	2.616, 2.623	[86]
<i>Bitetrahedral</i>					
[Au ₆ (PPh ₃) ₆](NO ₃) ₂ (3 NO ₃)	2.652–2.839 (2.759)	2.652	2.662, 2.669 ^b	–	[40]
[Au ₈ (dppp) ₄ Cl ₂](PF ₆) ₂ (11 ·PF ₆)	2.648–2.872 (2.775)	2.648	2.650, 2.658 ^a	2.970–3.072	[81]
[Au ₈ (dppp) ₄ (C≡CPh) ₂](NO ₃) ₂ (12 ·NO ₃)	2.628–2.865 (2.786)	2.628	2.666 ^a	2.932, 3.019	[91]
[Au ₈ (dppa) ₄ Cl ₂](Cl ₂) (13 ·Cl)	2.619–2.814 (2.728)	2.619	2.621 ^a	2.974–3.052	[96]
<i>Tri-tetrahedral</i>					
[Au ₈ (dppp) ₄](NO ₃) ₂ (9 NO ₃)	2.607–2.896 (2.790)	2.630	2.607 ^b	–	[81]
[Au ₆ (xy-xantphos) ₃](Cl) (5 ·Cl)	2.653–3.105 (2.779)	2.653 ^c		–	[77]

^a*Exo*-bridged edges

^bEdges not containing gold atoms shared by two or more Au₄ tetrahedra

^cThe edge shared by three Au₄ tetrahedra

In contrast to the diverse geometries of hexanuclear clusters, pentagonal bipyramid is the only one geometry known for Au₇ clusters (**6**). The distances between the two vertexes are extremely short in the range 2.561–2.581 Å.

4.3 Exo-attached Polyhedral Clusters (core+exo Type)

As described in the previous sections, assembling of gold atoms intrinsically favors to form polyhedral skeletons. However, some clusters adopt unusual geometries with extra gold atoms located outside the polyhedral core (“core+exo” type), especially when coupled with bidentate phosphine ligand. The first example reported by van der Verden et al. in 1979 is [Au₅(dppm)₃(dppm-H)]²⁺ (**1**), which has a tetrahedral Au₄ core and an additional gold atom outside the tetrahedron [23]. The second example is “blue” Au₆ cluster ([Au₆(dppp)₄]²⁺, **4**) reported by van der Verden et al. in 1982 [26]. The single-crystal structure shows this cluster contains a tetrahedral Au₄ core and two gold atoms bridged at opposite edges of the tetrahedron, thus being described as an Au₄+2Au type structure. Each of the gold atoms forming the central tetrahedron is coordinated by a single phosphine ligand, while the gold atoms at the *exo* positions accommodate two phosphine ligands. The core-to-*exo* distances (distances of *exo* gold atom from bonded gold atoms in the polyhedral core) are 2.798 Å, which fall in the typical distance range of PGCs (Table 3). For a long time, these have been supposed to be unusual cases, but we have recently reported higher-nuclearity clusters with similar structural features (**11**, **12**, **32** in Fig. 5).

[Au₈(dppp)₄Cl₂]²⁺ (**11**) has an edge-sharing bi-tetrahedral Au₆ core with two *exo* gold atoms bridged on the terminal edges of the bitetrahedron, thus being viewed as an extended version of **4**. The two chloride ligands, each of which is bonded to one of the terminal gold atoms, are forced to be oriented in *trans* configuration because of the chelation restriction by the dppp ligands. The bitetrahedral Au₆ core shows distances of the shared edge of 2.648 Å and the bridged terminal edges of 2.666 Å, which are nearly identical to those of [Au₆(PPh₃)₆]²⁺ (**3**) (2.652 and 2.666 Å) and are evidently shorter than the other Au–Au bonds (2.779–2.872 Å) (Table 3) [40]. On the other hand, the core-to-*exo* distances are in the range 2.970–3.072 Å, which are markedly longer than Au–Au distance in the bitetrahedral core (2.648–2.872 Å). Other Au₆+2Au type clusters (**12** and **13**) were reported recently [91, 96], which show almost similar structural parameters (Table 4).

We have also recently synthesized a new dodeca-coordinated Au₁₁ cluster [Au₁₁(dppe)₆]³⁺ (**32**) (Au₁₁P₁₂ type) [74]. Unlike conventional deca-coordinated Au₁₁L₁₀ clusters with polyhedral-only geometries (**23**–**31**), **32** has a core+*exo* type geometrical feature. Its polyhedral core is a butterfly-shaped Au₉, which resembles the Au₉ core of **14a**, **15**, and **16a**. The *exo* atoms form triangles by sharing an edge of the Au₉ core. Each of the *exo* gold atoms is bonded to the two phosphine ligands, whereas the eight peripheral gold atoms of the Au₉ core accommodate single

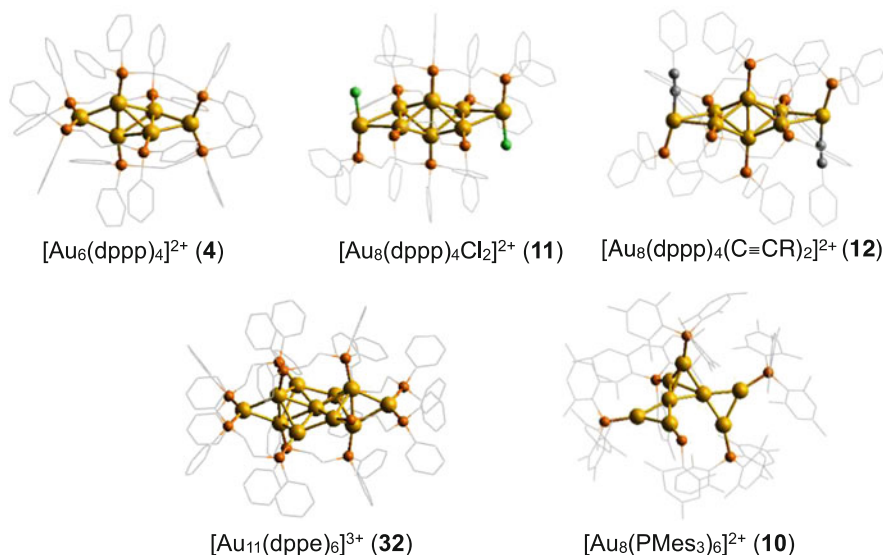


Fig. 5 Single-crystal X-ray structures of clusters having a polyhedral core with *exo*-attached gold atoms. Counter anion: NO_3 (**4**, **12**), PF_6 (**11**), BF_4 (**10**), SbF_6 (**32**)

Table 4 Au–Au bond distances (Å) of butterfly-shaped Au_9 unit of $[\text{Au}_9(\text{PPh}_3)_8]^{3+}$ (**14a**) and that of Au_9+2Au type Au_{11} cluster $(\text{Au}_{11}(\text{dppe})_6)^{3+}$, **32**)

	Mean dist. of Au_9 unit	Radial	Peripheral	<i>exo</i> -to-core	References
$[\text{Au}_9(\text{PPh}_3)_8](\text{NO}_3)_3$ (14a · NO_3)	2.777	2.675–2.708 (2.691)	2.762–2.880 (2.834)	–	[62]
$[\text{Au}_{11}(\text{dppe})_6]$ (SbF_6) ₃ (32 · SbF_6)	2.814	2.666–2.824 (2.745)	2.629–2.971 (2.860)	2.777, 2.824	[74]

phosphine ligands. The Au_9 core unit is apparently similar to previously known examples of butterfly-shaped clusters, although it has a slightly wider range of Au–Au bond distances (2.629–2.971 Å) than $[\text{Au}_9(\text{PPh}_3)_8]^{3+}$ (2.675–2.880 Å) (Table 4) [62]. Significantly, the *exo*-bridged edges are very short (2.629 Å) compared with the shortest peripheral–peripheral bonds of the non-*exo* type clusters (i.e., 2.762 Å for **14a**· NO_3). This may reflect some distortion caused by the bridging of the *exo* gold atoms. The core-to-*exo* distances were 2.777 and 2.824 Å, which lie in the range of the bond distances in the central butterfly unit.

These core+*exo* type clusters exhibit impressive colors that are different from conventional centered polyhedral clusters. This aspect will be mentioned in the next section. Among the three core+*exo* type clusters (Au_6 , Au_8 , Au_{11}), Au_8 clusters (**11–13**) are different in the context that they have additional anionic ligands (sub-ligands). The long *exo*-to-core distance in **11–13** can be attributed to the

electron-withdrawing character of the anionic ligands attached to the *exo* gold atoms, which may weaken the Au–Au interaction between the *exo* Au atoms and the central Au₆ unit [101]. This is noteworthy in comparison with the short Au–AuCl distances in Au₁₃ clusters [34].

As a different core+*exo* type geometry, Sharp et al. reported Au₈ cluster coordinated by sterically hindered monophosphines ([Au₈(PMes₃)₆]²⁺ (**10**) [86]. This cluster has a tetrahedral core with edge distances of 2.697–2.711 Å, where two triangles are attached to the adjacent tetrahedral vertexes. The *exo*-to-core distances (2.616 and 2.623 Å) are slightly shorter than the tetrahedron edges.

5 Optical Properties

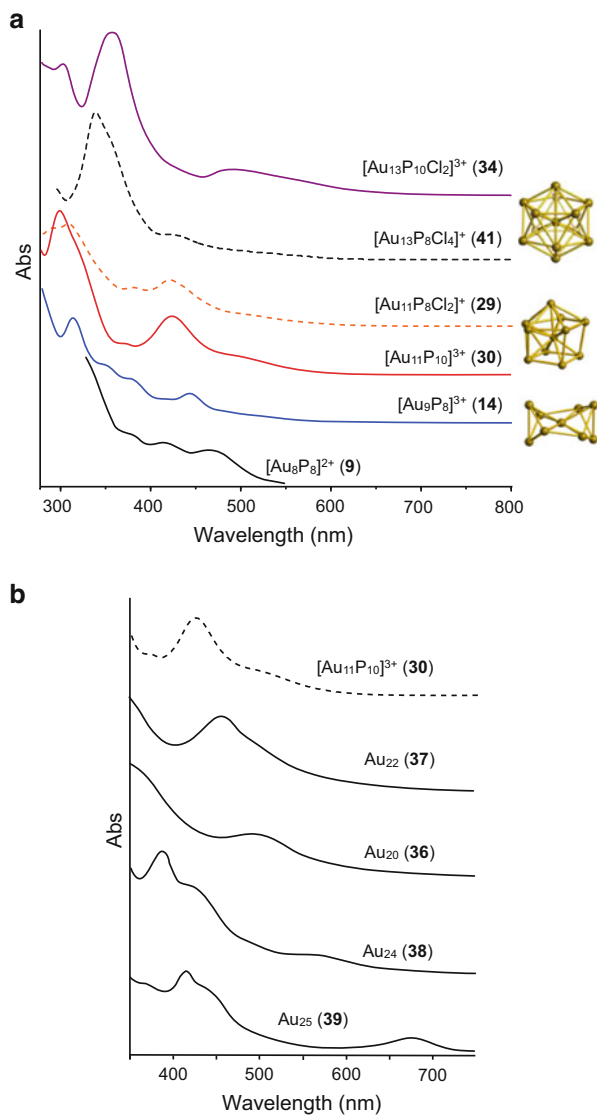
5.1 Electronic Absorption Spectra

Generally PGCs are highly colored, so UV–visible electronic absorption spectra have been widely utilized for characterization. Unlike well-known red colors of large gold colloids (sizes of ~2 nm or above) offered by localized surface plasmon, the colors of ultrasmall gold clusters including PGCs essentially originate from the discrete electronic transitions, which is supported theoretically [102]. Therefore, the absorption spectra are useful not only for characterization but also to obtain insights into the electronic structures of cluster compounds. On the other hand, in the nano-size regime, it is well accepted that the lowest optical transition energy of metal atom assemblies increases as the size is reduced, which is known as quantum-size effects. In this relation, studies on the relationship between the nuclearity and the absorption spectra would provide useful knowledge about the intermediate between nano-objects and molecules.

5.1.1 Centered Polyhedral Clusters

Solution absorption spectra of Au₈P₈ (**8**·BF₄), Au₉P₈ (**14**·NO₃), Au₁₁P₈Cl₂ (**29**·Cl) Au₁₁P₁₀ (**30**·NO₃), Au₁₃P₁₀Cl₂ (**34**·Cl), and Au₁₃P₁₀Cl₂ (**41**·Cl) clusters, which adopt centered polyhedral geometries, are shown in Fig. 6a. The spectra except **8**·BF₄ were measured in our laboratory for crystallographically characterized or equivalently pure samples. The spectrum of **8**·BF₄ is from the literature [34]. The spectral data together with those in literatures are summarized in Table 5. As a common feature, these centered polyhedral clusters exhibit tail-and-humps spectral characteristics, in which relatively weak visible absorption bands are overlapped with the main band in the UV region tailing to the red. For example, Au₉P₈ cluster (**14**) shows the lowest energy visible band at ~450 nm and more intense UV band at ~315 nm. Au₁₁ clusters ([Au₁₁P₈Cl₂]⁺ (**29**) and [Au₁₁P₁₀]³⁺ (**41**)) show sets of a visible band at ~420 nm and more intense UV bands at ~300 nm. The spectral

Fig. 6 Absorption spectra of selected centered clusters at ambient temperature. For solvents and counter ions (see Table 5)



patterns of the other [Au₁₁P₁₀]³⁺ clusters (**31** and **31'**) and neutral Au₁₁P₇Cl₃ cluster (**29'**) are essentially similar (Table 5) [65, 71], so they seem to be unaffected by the associated surface ligands, cluster charge, and counter anions.

For Au₁₃ clusters, Mingos et al. have reported that [Au₁₃(PMe₂Ph)₁₀Cl₂]³⁺ (**33**, Au₁₃P₁₀Cl₂ type) and [Au₁₃(PMePh₂)₁₀Cl₄] (**33'**, Au₁₃P₈Cl₄ type) clusters give almost identical spectra in DCM with intense UV band at ~340 and a smaller hump (shoulder) at ~430 nm. From this observation, they concluded that the spectra is solely dependent on the nuclearity but is far less so on the surrounding ligands

Table 5 Electronic absorption and photoluminescence spectral data of crystallographically characterized centered PGCs and related clusters^a

N	Cluster formula	Solvent	Abs bands (nm) ^b	ϵ (M ⁻¹ cm ⁻¹)	PL λ_{em} (nm) ^c	References
8	[Au ₈ (PPH ₃) ₈](BF ₄) ₂ (8 ·BF ₄)	MeOH	460 412 370	nd	–	[34]
9	[Au ₉ (PPH ₃) ₈](NO ₃) ₂ (14 ·NO ₃)	MeOH	443 375 352 314	1.6×10^4 (443 nm)	NP	[34]
9	[Au ₉ (P[<i>p</i> -MeOC ₆ H ₄] ₃) ₈](BF ₄) ₃ (16 ·BF ₄)	DCM	456 379 342 316	1.6×10^4 (456 nm)	nd	[34]
11	[Au ₁₁ (PPH ₃) ₈ Cl ₂](Cl) (29 ·Cl) ^e	MeOH	~500 (sh) 421 380 308	4.0×10^4 (421 nm)	NP	[69]
11	[Au ₁₁ (dppp) ₅](NO ₃) ₃ (30 ·NO ₃)	DCM	~500 (sh) 425 370 301	nd	NP	[69]
11	[Au ₁₁ (PMePh ₂) ₁₀](BPh ₄) ₃ (31 ·BPh ₄) ^e	DCM	422 374, 298	2.2×10^4 (422 nm)	nd	[34]
11	[Au ₁₁ (PMePh ₂) ₁₀](CB) ₃ (31 ·CB) ^d	DCM	425 378 302	3.8×10^4 (425 nm)	nd	[42]
11	[Au ₁₁ (PMe ₂ Ph) ₁₀](BPh ₄) ₃ (31' ·BPh ₄) ^e	DCM	412, 368, 293	3.0×10^4 (412 nm)	nd	[34]
13	[Au ₁₃ (PMe ₂ Ph) ₁₀ Cl ₂](PF ₆) ₃ (33 ·PF ₆)	DCM	428 338	1.0×10^5 (338 nm)	nd	[34]
13	[Au ₁₃ (PMePh ₂) ₈ Cl ₄](CB) ^e (33' ·CB)	DCM	425 (sh) 341	1.2×10^5 (341 nm)	nd	[43]
13	[Au ₁₃ (dppp) ₅ Cl ₂](Cl ₃) (34 ·Cl)	MeCN	493 359 304	9.3×10^4 (359 nm)	766	[75]
13	[Au ₁₃ (dppp) ₄ Cl ₄](Cl) (41 ·Cl) ^e	MeCN	430 340	nd	~780	[76]
20	[Au ₂₀ (PPh[4-Py] ₂) ₁₀ Cl ₄](Cl ₂) (36 ·Cl)	DCM	493 344(sh)	nd	nd	[66]
22	Au ₂₂ (dppo) ₆ (37)	DCM	456	nd	~700	[73]
24	[Au ₂₄ (PPh ₃) ₁₀ (SC ₂ H ₄ Ph) ₅ X ₂] ⁺ (38)	DCM	560 383	nd	~818 ^f	[79]
25	[Au ₂₅ (PPh ₃) ₁₀ (SEt) ₅ Cl ₂] ²⁺ (39)	DCM	670, 415	nd	~1000	[85]

^aNP no photoluminescence, nd no data given^bShown for the bands at >290 nm^cExcitation at lowest-energy absorption band^dCB: C₂B₉H₁₂^eNot identified by single-crystal X-ray diffraction but the purity was checked by mass spectral and/or elemental analyses^f λ_{ex} = 500 nm

(P:Cl ratio). We observed similar spectral patterns for $[\text{Au}_{13}(\text{dppp})_4\text{Cl}_4]^+$ (**41**, $\text{Au}_{13}\text{P}_8\text{Cl}_4$ type) in MeCN (Fig. 6a) and in DCM [76]. On the other hand, the spectrum of $[\text{Au}_{13}(\text{dppe})_5\text{Cl}_2]^{3+}$ (**34**, $\text{Au}_{13}\text{P}_{10}\text{Cl}_2$ type) in MeCN is markedly different, showing a main band at ~ 360 nm together with a broad weaker band at ~ 500 nm (Fig. 6a) [75]. Therefore, for the diphosphine-coordinated series, the absorption profiles are critically dependent on the number of Cl ligand ratio, suggesting the involvement of the ligand-mediated transitions in the observed electronic absorptions.

The spectra of higher-nuclearity centered clusters (**36–39**) taken from the literatures [66, 73, 79, 85] are summarized in Fig. 6b. They all exhibit tail-and-humps profiles. There seems no relationship between the nuclearity and the positions of the lowest-energy visible bands, and the transitions are interpreted in individual cases. For **36** and **37**, whose structures can be viewed as the dimers of the icosahedron-based Au_{11} clusters, the visible bands are observed at lower energies than that of the parent cluster. For **39**, the exceptionally low-energy band (680 nm) is noteworthy, which suggests the effective electronic interaction between two Au_{13} cluster units via vertex sharing.

5.1.2 Non-centered and Core+*exo* Clusters

Figure 7 shows the solution absorption spectra of edge-sharing bitetrahedral Au_6P_6 cluster (**3**· NO_3), tritetrahedral Au_8P_6 cluster (**9**· NO_3), and [core+*exo*]-type Au_6P_8 (**4**· NO_3) $\text{Au}_8\text{P}_8\text{Cl}_2$ (**11**·Cl), and $\text{Au}_{11}\text{P}_{12}$ (**32**· SbF_6) clusters, together with the spectra of centered toroidal Au_9P_8 (**14**· NO_3) and spherical $\text{Au}_{11}\text{P}_{10}$ (**30**· NO_3) clusters for comparison. Except the spectrum of **6**, which is taken from the literature [34], all spectra were measured in our laboratory and the sample purity was checked by ESI-MS and NMR. The spectral data are summarized in Table 6. Similarly to the above-mentioned cases of centered polyhedral core-only clusters, the spectrum of the bitetrahedral cluster (**3**) can be described as the combination of intense UV bands and relatively weak visible bands. However, the visible bands at 452 and 476 nm are considerably separated from the UV bands. A similar trend was observed for the edge-sharing trimer of the tetrahedral Au_4 motif (**9**). The spectrum showed a band at 520 nm together with a smaller shoulder band at ~ 590 nm, which are completely separated from the UV band at 308 nm. At the present stage, these transitions are not assigned, but seem to be a common feature of edge-sharing tetrahedral clusters. The low energies of the visible absorptions of the trimer (**9**) when compared with the dimer (**3**) can be attributed to the simple mixing of MOs of the tetrahedral-based units (bitetrahedron and tetrahedron).

[Core+*exo*]-type clusters having edge-sharing gold triangle moieties exhibit more distinctive spectral features. For example, Au_4+2Au type Au_6P_8 (**4**), Au_6+2Au type $\text{Au}_8\text{P}_8\text{Cl}_2$ (**11**), and Au_9+2Au type $\text{Au}_{11}\text{P}_{12}$ (**32**) all showed single visible bands at 587, 508, and 663 nm, respectively, which are fairly separated from the short-wavelength bands spreading into the UV regions. These spectra are much different in pattern from the tail-and-humps feature of centered only-polyhedral

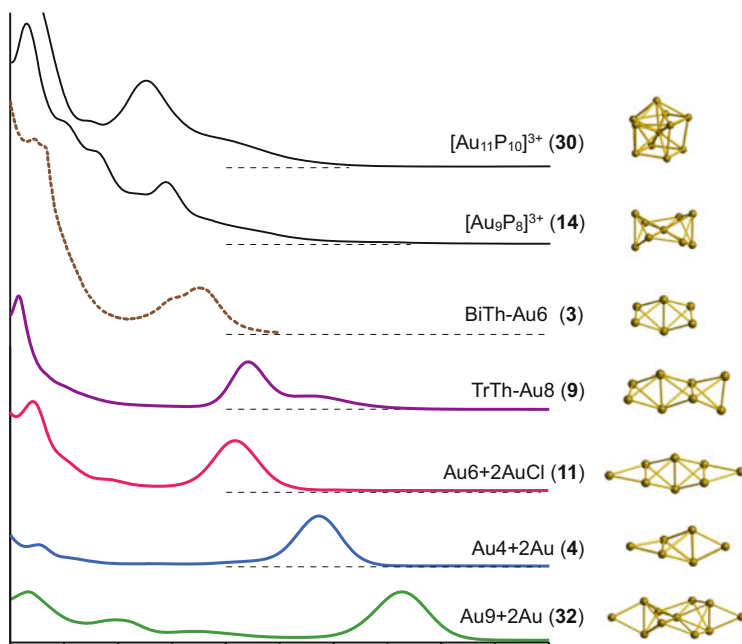


Fig. 7 Solution absorption spectra of selected non-centered and core+*exo* clusters at ambient temperature. For conditions and counter ions (see Table 5)

clusters such as toroidal Au_9P_8 cluster (**14**) and spherical Au_{11}P_8 cluster (**30**). Therefore, the “isolated” absorption bands are likely a common feature of [core+*exo*] type clusters. The attachment of extra gold atoms to the polyhedral core may allow the generation of new electronic structures that are associated with the characteristic visible absorptions. Actually the absorption bands of **32** did not coincide with any bands of $[\text{Au}_9(\text{PPh}_3)_8]^{3+}$ (**14**), which has a toroidal core and thus can be a model of the central substructure of **32**. It should also be noted that the lowest transition energy increased in the order Au_{11} (**32**, 1.87 eV) < Au_6 (**4**, 2.11 eV) < Au_8 (**11**, 2.44 eV), not matching the order of nuclearity. Furthermore, noticeable differences in the spectral profiles are found between the isomeric structures of Au_6 (**3** vs **4**), Au_8 (**8** vs **9** vs **11**), and Au_{11} (**30** vs **32**). Therefore, the optical properties of these clusters depend more strongly on geometric structure than on nuclearity.

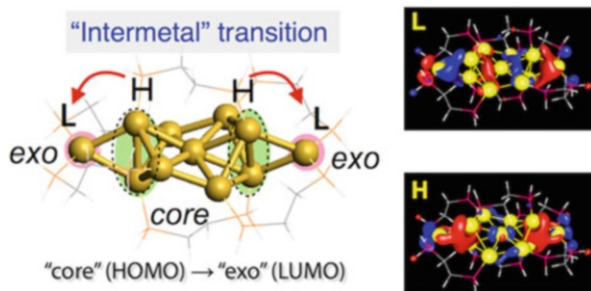
Table 6 summarizes the spectra data of the tetrahedron-based and core+*exo* type clusters. For the core+*exo* series, the ϵ values of the all-phosphine type clusters (**3** and **32**) are noticeably larger than those of **8** and **9** with anionic ligands, which may be correlated with the long core-to-*exo* distances (Tables 3 and 4). Density functional theory (DFT) studies on corresponding non-phenyl models of **3**, **8**, and **30** show that they have similar electronic structures with discrete HOMO and LUMO bands, which are predominantly constituted by $\text{Au}(6\text{sp})$ orbitals (sp bands) and are appreciably separated from the closest orbitals. The theoretical

Table 6 Electronic absorption spectral data of non-centered and core+exo type PGCs^{a, b}

<i>N</i>	Cluster formula	Structure type	Abs bands (nm)	ϵ ($M^{-1} cm^{-1}$)	PL λ_{em} (nm) ^d	References
6	[Au ₆ (PPh ₃) ₆](NO ₃) ₂ (3 ·NO ₃)	Bitetrahedral	476 452 330 319	nd	nd	[34]
8	[Au ₈ (dppp) ₄](NO ₃) ₂ (9 ·NO ₃)	Tritetrahedral	590 (sh) 520 308	3.0×10^4 (520 nm)	NL	[81]
6	[Au ₆ (dppp) ₄](NO ₃) ₂ (4 ·NO ₃)	Au ₄ +2Au	587 432 326 ^c	8.9×10^4 (587 nm)	nd ^e	[101]
8	[Au ₈ (dppp) ₄ Cl ₂](Cl) ₂ (11 ·Cl)	Au ₆ +2Au	508 390 322	2.7×10^4 (508 nm)	597	[81]
8	[Au ₈ (dppp) ₄ (C≡CPh) ₂](NO ₃) ₂ (12 ·NO ₃)	Au ₆ +2Au	509 393 325	3.9×10^4 (509 nm)	577	[91]
11	[Au ₁₁ (dppe) ₆](SbF ₆) ₃ (32 ·SbF ₆)	Au ₉ +2Au	663 471 390 316	8.9×10^4 (663 nm)	nd ^e	[74]

^aNL non-luminescent, nd no data given^bIn DCM at room temperature unless otherwise noted. Almost identical spectra were obtained in MeCN and MeOH^cIn MeOH^dExcited at the lowest-energy absorption band^eEssentially PL active (Fig. 9b)

Fig. 8 Schematic illustration of HOMO and LUMO of $[\text{Au}_{11}(\text{dppe})_6]^{3+}$ (**32**)



spectra generated by time-dependent DFT (TD-DFT) calculations reproduce well the experimental spectra, leading to the assignment of the characteristic visible bands to intermetal HOMO–LUMO transitions. Orbital distribution analyses demonstrate the HOMO and LUMO are both found in proximity to the terminal Au_3 triangles containing the *exo* gold atom, and the HOMO→LUMO transition occurs in the core→*exo* direction (Fig. 8).

5.1.3 Summary

Electronic absorption properties of PGCs are strictly dependent not only on the nuclearity but also on the geometrical structures of the cluster units. Centered polyhedral-only clusters generally show tail-and-humps spectra, while tetrahedron-based and [core+*exo*]-type clusters give isolated absorption bands in the visible region. Except some exceptions, the spectral profiles are essentially defined by the nuclearity/geometry of the gold cluster units, and the modification of the surface ligands cause little effects on the spectral pattern. The transition energies (band positions) show no clear correlation with the order of nuclearity and vary significantly with the individual arrangements of gold atoms, indicating the strong “molecular” characters of this class of cluster compounds.

5.2 Photoluminescence

In recent years there has been intense interest in the luminescence properties of ultrasmall noble metal clusters due to their potential utility as quantum dots [13]. However, the origin of the luminescence has not been elucidated yet because of the lack of the geometrical information. Ligand-coordinated ultrasmall gold clusters including PGCs are potentially photoluminescent due to the small size, but there have been very limited studies. We found that $[\text{Au}_9(\text{PPh}_3)_8]^{3+}$ (**14**) and $[\text{Au}_{11}\text{L}_{10}]^{3+}$ clusters (**29**, **29'** and **30**) are virtually PL inactive. In contrast, $\text{Au}_{13}\text{P}_{10}\text{Cl}_2$ cluster **34** is appreciably photoluminescent, giving a PL band in the near IR region (766 nm) when excited at 500 nm, with a moderately high quantum

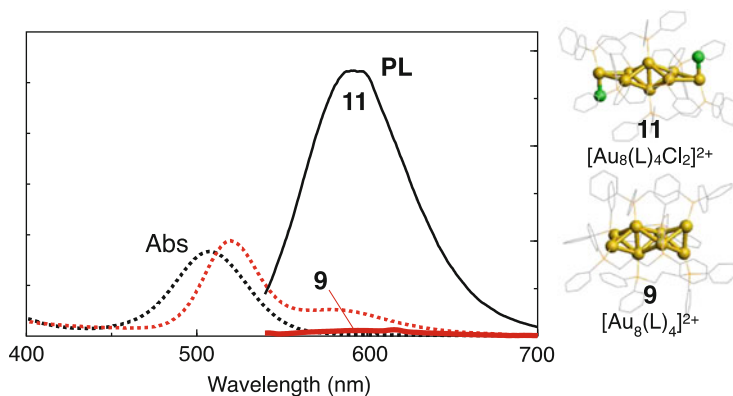


Fig. 9 Absorption (dotted lines) and PL (solid lines) spectra of two isomeric forms of Au_8 clusters: **9**- NO_3 (red) and **11**-Cl (black) in MeOH at 25°C

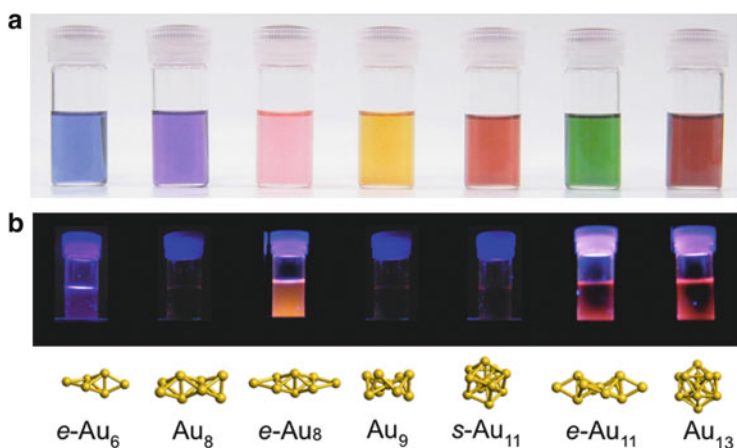


Fig. 10 Pictures of solution samples of PGCs (a) under room light and (b) under irradiation of a 365-nm handy UV lamp. (Left to right) $[\text{Au}_6(\text{dppp})_4](\text{NO}_3)_2$ (**4**- NO_3); $[\text{Au}_8(\text{dppp})_4](\text{NO}_3)_2$ (**9**- NO_3); $[\text{Au}_8(\text{dppp})_4\text{Cl}_2](\text{Cl})_2$ (**11**-Cl); $[\text{Au}_9(\text{PPh}_3)_8](\text{NO}_3)_2$ (**14**- NO_3); $[\text{Au}_{11}(\text{PPh}_3)_8\text{Cl}_2]\text{Cl}$ (**29**-Cl); $[\text{Au}_{11}(\text{dppe})_6](\text{SbF}_6)_3$ (**32**- SbF_6); $[\text{Au}_{13}(\text{dppe})_5\text{Cl}_2]\text{Cl}_3$ (**34**-Cl)

yield (0.076) [75]. On the other hand, the $\text{Au}_{13}\text{P}_8\text{Cl}_4$ cluster **41** shows a PL band at a similar wavelength but the quantum efficiency is considerably small (0.008), indicating that the local environment (ligand) in proximity to the gold core notably affects the radiative path that contributes the PL emission.

We have also found that [core+exo]-type Au_6 , Au_8 , and Au_{11} clusters are essentially PL active (Fig. 10b). For example, $[\text{Au}_8(\text{dppp})_4\text{Cl}_2]^{2+}$ (**11**) shows an evident photoluminescence band at 597 nm upon excitation at 509 nm (Fig. 9, black solid line). The excitation spectrum monitored at 600 nm almost coincided with the absorption spectrum. Similarly to the abovementioned Au_{13} clusters, the PL profiles

of the core+*exo* type Au₈ clusters appear to be notably affected by the sub-ligand (e.g., Cl in **11**). [Au₈(dppp)₄(C≡CPh)₂](NO₃)₂ (**12**·NO₃), which has two acetylide units in place of chloride ligands, shows a similar PL band at a noticeably higher energy (577 nm). On the other hand, [Au₈(dppp)₄](NO₃)₂ (**9**·NO₃) having a tetrahedron trimer motif, which is isomeric to that of **11** and **12**, was almost PL inactive (red solid line), again indicating that the optical properties of PGCs are strictly dependent on their geometries.

5.3 Gold Clusters as Stimuli-Responsive Chromic Modules

As expected from the visible absorption profiles mentioned above, PGCs exhibit a wide variety of colors ranging over the whole visible region. Figure 10 shows the pictures of the solution samples of representative clusters under room light and UV-light, which reveal that their colors and PL activities are highly dependent on the number (nuclearity) and arrangement (geometry) of the gold atoms. Especially, the colors of the core+*exo* type clusters are impressive; their blue, pink, and green colors are unusual for gold clusters, which are markedly different from the plasmon-like reddish colors of conventional centered clusters such as Au₉, Au₁₁, and Au₁₃. This is surprising in the sense that the components of the clusters are virtually same and the optical property is simply governed by the arrangement of the gold atoms. The subtle difference in the arrangement leads to the great color differences.

In this context, one of the prominent features of gold clusters is their soft potential energy surfaces. This potentially allows the reversible interconversion among several particular geometries, through which the optical properties of the clusters would be altered. This idea can be supported by the earlier work by Mingos et al., who provide an example of the color and reflectance spectral difference between the butterfly and crown isomers of Au₉ cluster in the solid state [38]. Thus, if the cluster geometry can be tuned by external stimuli, one would see the optical responses in color change or PL on–off. Therefore, these gold clusters have a unique potential to serve as stimuli-responsive chromism modules and may be applied to chemical sensors.

As an example, we have recently shown a redox-induced chromism system based on the isomerization of the Au₈ units between **9** and **11** (Fig. 11) [81]. Thus, the formal charges of the Au₈ units of **9** and **11** were 2+ and 4+, respectively, which can be reversibly converted into each other via two-electron redox processes. As noted in the previous sections, the reduced form (**9**) is violet in color and PL inactive, whereas the oxidized form (**11**) is pink in color and PL active. As shown in Fig. 10, it is possible to switch the optical properties reversibly (color and PL) through chemical reduction/oxidation. The use of electrochemical processes would also be feasible, so the present cluster system has the potential for redox-based functions such as electrochromism.

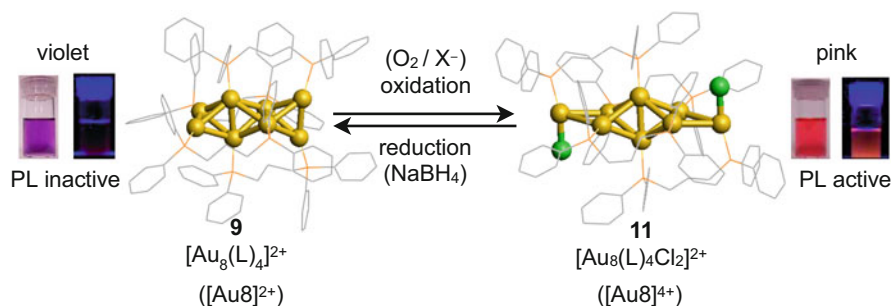


Fig. 11 Redox-mediated chromism between **9** and **11** associated with the isomerization of the Au₈ cluster framework



Fig. 12 Protonation-induced chromism of 4-pyridylethynyl-appended Au₈ cluster

Based on the general trend of the optical properties mentioned above, it is obvious that the nuclearity and geometries are primary factors to govern the optical properties of molecular gold clusters. In addition, the alteration of nearby or external environments or physical stimuli could affect the optical properties, but such aspects have not been explored. We have recently found that the electronic perturbation coupled with π -conjugated system actually affects the optical properties of the cluster units [91]. As shown in Fig. 12, the [core+*exo*]-type Au₈ clusters bearing two pyridylethynyl ligands on the *exo* gold atoms ($[\text{Au}_8(\text{dppp})_4(\text{C}\equiv\text{C}(\text{Py}))_2]^{2+}$) exhibit reversible visible absorption and photoluminescence responses to protonation/deprotonation events of the terminal pyridyl moieties. It is demonstrated that the chromism behaviors are highly dependent on the relative position of the pyridine nitrogen atom. Therefore the formation of extended charged resonance structures upon pyridine protonation causes significant perturbation effects on the electronic properties of the Au₈ unit. This is an example in which organic π -conjugated system and inorganic gold cluster are electronically combined, providing an implication for the design of cluster-based stimuli-responsive chromic modules.

6 Concluding Remarks

In the present chapter, the syntheses, X-ray structures (geometries), and optical properties of phosphine-coordinated molecular gold clusters (PGCs) have been summarized. The inspection of the optical properties in the context of the geometrical structures reveals a strong molecular character of PGCs. In addition to the conventional clusters discovered more than 30 years ago, several new families with unique geometrical and optical features have now been identified, thereby expanding the scope of this class of compounds. Among them, unusual optical properties of a series of [core+exo]-type clusters are quite interesting, which demonstrates that the attachment of only one or two gold atoms to polyhedral cores dramatically changes the electronic structures of total metal entities. This principle would be applicable to the colloidal system, which will benefit the rational design of functional colloids. It has been demonstrated that the use of bidentate ligands occasionally allows the generation of unusual cluster species, but it is still at a phenomenological level. The computer-aided design of multidentate phosphines would promote the emergence of unique PGCs. Finally, as shown in the last topic, the electronic structures (optical properties) of PGCs can be altered not only by the geometrical parameters but also by the electronic perturbation by the external stimuli. The combination with appropriate organic units as well as the design/discovery of novel skeletons would lead to the evolution of PGCs to functional materials.

Acknowledgments The author is grateful to Professor Michael Mingos for reading the drafts of this chapter and providing useful comments, and to Dr. Yutaro Kamei for his help in preparing graphics and also checking the structural and spectral data.

References

1. Daniel M-C, Astruc D (2004) Gold nanoparticles: assembly, supramolecular chemistry, quantum-size-related properties, and applications toward biology, catalysis, and nanotechnology. *Chem Rev* 104(1):293–346
2. Fernandez EJ, Monge M (2008) Gold nanomaterials. In: Laguna A (ed) *Modern supra molecular gold chemistry: gold-metal interactions and applications*. WILEY-VCH, Weinheim, pp 131–179. doi:10.1002/9783527623778.ch3
3. Sardar R, Funston A, Mulvaney P, Murray R (2009) Gold nanoparticles: past, present, and future. *Langmuir* 25(24):13840–13851
4. Giljohann D, Seferos D, Daniel W, Massich M, Patel P, Mirkin C (2010) Gold nanoparticles for biology and medicine. *Angew Chem Int Ed* 49(19):3280–3294
5. Takei T, Akita T, Nakamura I, Fujitani T, Okumura M, Okazaki K, Huang J, Ishida T, Haruta M (2012) Heterogeneous catalysis by gold. *Adv Catal* 55:1–126
6. Hutchings GJ, Edwards JK (2012) Application of gold nanoparticles in catalysis. Metal nanoparticles and nanoalloys. In: Johnstone RL, Wilcoxon JP (eds) *Frontiers of nanoscience*, vol 3. Elsevier, Oxford, pp 249–293

7. Wilson R (2008) The use of gold nanoparticles in diagnostics and detection. *Chem Soc Rev* 37(9):2028–2045
8. Bai C, Liu M (2013) From chemistry to nanoscience: not just a matter of size. *Angew Chem Int Ed* 52(10):2678–2683
9. Lu Y, Chen W (2012) Sub-nanometre sized metal clusters: from synthetic challenges to the unique property discoveries. *Chem Soc Rev* 41(9):3594–3623
10. Tsukuda T (2012) Toward an atomic-level understanding of size-specific properties of protected and stabilized gold clusters. *Bull Chem Soc Jpn* 85(2):151–168
11. Jin R (2010) Quantum sized, thiolate-protected gold nanoclusters. *Nanoscale* 2(3):343–362
12. Häkkinen H (2012) The gold-sulfur interface at the nanoscale. *Nat Chem* 4(6):443–455
13. Zheng J, Nicovich P, Dickson R (2007) Highly fluorescent noble-metal quantum dots. *Ann Rev Phys Chem* 58:409–431
14. Jadzinsky P, Calero G, Ackerson C, Bushnell D, Kornberg R (2007) Structure of a thiol monolayer-protected gold nanoparticle at 1.1 Å resolution. *Science* 318(5849):430–433
15. Heaven MW, Dass A, White PS, Holt KM, Murray RW (2008) Crystal structure of the gold nanoparticle $[\text{N}(\text{C}_8\text{H}_{17})_4][\text{Au}_{25}(\text{SCH}_2\text{CH}_2\text{Ph})_{18}]$. *J Am Chem Soc* 130(12):3754–3755
16. Zhu M, Eckenhoff WT, Pintauer T, Jin R (2008) Conversion of anionic $[\text{Au}_{25}(\text{SCH}_2\text{CH}_2\text{Ph})_{18}]^-$ Cluster to charge neutral cluster via air oxidation. *J Phys Chem C* 112(37):14221–14224
17. Zhu M, Aikens C, Hollander F, Schatz G, Jin R (2008) Correlating the crystal structure of a thiol-protected Au_{25} cluster and optical properties. *J Am Chem Soc* 130(18):5883–5885
18. Qian H, Eckenhoff W, Zhu Y, Pintauer T, Jin R (2010) Total structure determination of thiolate-protected Au_{38} nanoparticles. *J Am Chem Soc* 132(24):8280–8281
19. Naldini L, Cariati F, Simonetta G, Malatesta L (1966) Gold? Tertiary phosphine derivatives with intermetallic bonds. *Chem Commun* 18:647
20. Vollenbroek FA, Bosman WP, Bour JJ, Noordik JH, Beurskens PT (1979) Reactions of gold? phosphine cluster compounds. Preparation and X-ray structure determination of octakis (triphenylphosphine)octa-gold bis(hexafluorophosphate). *J Chem Soc Chem Commun* (9):387–388
21. Vollenbroek FA, Bour JJ, van der Veden JWA (1980) Gold-phosphine cluster compounds: The reactions of $[\text{Au}_9\text{L}_8]^{3+}$ ($\text{L}=\text{PPh}_3$) with L , SCN^- and Cl^- to $[\text{Au}_8\text{L}_8]^{2+}$ ($\text{Au}_{11}\text{L}_8(\text{SCN})_2$) $^+$ and $[\text{Au}_{11}\text{L}_8\text{Cl}_2]^{+}$. *Recl Trav Chim Pays Bas* 99(4):137–141
22. van der Velden JWA, Bour JJ, Bosman WP, Noordik JH (1981) Synthesis and X-ray crystal structure determination of the cationic gold cluster compound $[\text{Au}_8(\text{PPh}_3)_7](\text{NO}_3)_2$. *J Chem Soc Chem Commun* 23:1218–1219
23. van der Velden JWA, Vollenbroek FA, Bour JJ, Beurskens PT, Smits JMM, Bosman WP (1981) Gold clusters containing bidentate phosphine ligands. Preparation and X-Ray structure investigation of $[\text{Au}_5(\text{dppmH})_3(\text{dppm})](\text{NO}_3)_2$ and $[\text{Au}_{13}(\text{dppmH})_6](\text{NO}_3)_n$. *Recl Trav Chim Pays Bas* 100(4):148–152
24. Vollenbroek FA, van der Velden JWA, Bour JJ, Trooster JM (1981) Mössbauer investigation of gold cluster compounds. *Recl Trav Chim Pays-Bas* 100(10):375–377
25. Steggerda JJ, Bour JJ, Velden JWAvd (1982) Preparation and properties of gold cluster compounds. *Recl Trav Chim Pays Bas* 101:164–170
26. Van der Velden JWA, Bour JJ, Steggerda JJ, Beurskens PT, Roseboom M, Noordik JH (1982) Gold clusters. Tetraakis[1,3-bis(diphenylphosphino)propane]hexagold dinitrate: preparation, X-ray analysis, and gold-197 Moessbauer and phosphorus-31{proton} NMR spectra. *Inorg Chem* 21(12):4321–4324
27. Smits JMM, Beurskens PT, Bour JJ, Vollenbroek FA (1983) X-ray analysis of octakis(tri-*p*-tolylphosphine) enneagoldtris(hexafluorophosphate), $[\text{Au}_9\{\text{P}(p\text{-MeC}_6\text{H}_4)_3\}_8](\text{PF}_6)_3$: a redetermination. *J Cryst Spect Res* 13(5):365–372
28. Smits JMM, Beurskens PT, Velden JWA, Bour JJ (1983) Partial X-ray analysis of triiodoheptakis (triphenylphosphine)undecagold, $\text{Au}_{11}\text{C}_{126}\text{H}_{105}\text{I}_3\text{P}_7$. *J Cryst Spect Res* 13(5):373–379

29. Smits JMM, Bour JJ, Vollenbroek FA, Beurskens PT (1983) Preparation and X-ray structure determination of [pentakis{1,3-bis(diphenylphosphino)propane}] undecagoldtris(thiocyanate), $[\text{Au}_{11}\{\text{PPh}_2\text{C}_3\text{H}_6\text{PPh}_2\}_5](\text{SCN})_3$. *J Cryst Spect Res* 13(5):355–363
30. Van der Velden JWA, Bour JJ, Bosman WP, Noordik JH (1983) Reactions of cationic gold clusters with Lewis bases. Preparation and X-ray structure investigation of $[\text{Au}_8(\text{PPh}_3)_7](\text{NO}_3)_2 \cdot 2\text{CH}_2\text{Cl}_2$ and $\text{Au}_6(\text{PPh}_3)_4[\text{Co}(\text{CO})_4]_2$. *Inorg Chem* 22(13):1913–1918
31. Van der Velden JWA, Beurskens PT, Bour JJ, Bosman WP, Noordik JH, Kolenbrander M, Buskes JAKM (1984) Intermediates in the formation of gold clusters. Preparation and X-ray analysis of $[\text{Au}_7(\text{PPh}_3)_7]^+$ and synthesis and characterization of $[\text{Au}_8(\text{PPh}_3)_6\text{I}]\text{PF}_6$. *Inorg Chem* 23(2):146–151
32. van der Velden JWA, Bour JJ, Bosman WP, Noordik JH, Beurskens PT (1984) The electrochemical preparation of $[\text{Au}_9(\text{PPh}_3)_8]^+$. A comparative study of the structures and properties of $[\text{Au}_9(\text{PPh}_3)_8]^+$ and $[\text{Au}_9(\text{PPh}_3)_8]^{3+}$. *Recl Trav Chim Pays Bas* 103(1):13–16
33. Bos W, Kanters RPF, Van Halen CJ, Bosman WP, Behm H, Smits JMM, Beurskens PT, Bour JJ, Pignolet LH (1986) Gold clusters: synthesis and characterization of $[\text{Au}_8(\text{PPh}_3)_7(\text{CNR})]^{2+}$, $[\text{Au}_9(\text{PPh}_3)_6(\text{CNR}_2)]^{3+}$ and $[\text{Au}_{11}(\text{PPh}_3)_7(\text{CNR})_2\text{I}]^{2+}$ and their reactivity towards amines. The crystal structure of $[\text{Au}_{11}(\text{PPh}_3)_7(\text{CN-i-Pr})_2\text{I}](\text{PF}_6)_2$. *J Organomet Chem* 307(3):385–398
34. Hall KP, Mingos DMP (1984) Homo- and heteronuclear cluster compounds of gold. *Prog Inorg Chem* 32:237–325
35. Mingos DMP (1984) Gold cluster compounds. *Gold Bull* 17(1):5–12
36. Briant CE, Theobald BRC, White JW, Bell LK, Mingos DMP, Welch AJ (1981) Synthesis and X-ray structural characterization of the centred icosahedral gold cluster compound $[\text{Au}_{13}(\text{PMe}_2\text{Ph})_{10}\text{Cl}_2](\text{PF}_6)_3$; the realization of a theoretical prediction. *J Chem Soc Chem Commun* 5:201
37. Hall KP, Theobald BRC, Gilmour DI, Mingos DMP, Welch AJ (1982) Synthesis and structural characterization of $[\text{Au}_9\{\text{P}(\text{p-C}_6\text{H}_4\text{OMe})_3\}_8](\text{BF}_4)_3$; a cluster with a centred crown of gold atoms. *J Chem Soc Chem Commun* 10:528–530
38. Briant CE, Hall KP, Mingos DMP (1984) Structural characterisation of two crystalline modifications of $[\text{Au}_9\{\text{P}(\text{C}_6\text{H}_4\text{OMe-p})_3\}_8](\text{NO}_3)_3$; the first example of skeletal isomerism in metal cluster chemistry. *J Chem Soc Chem Commun* 5:290–292
39. Briant CE, Hall KP, Wheeler AC, Mingos DMP (1984) Structural characterisation of $[\text{Au}_{10}\text{Cl}_3(\text{PCy}_2\text{Ph})_6](\text{NO}_3)(\text{Cy}=\text{cyclohexyl})$ and the development of a structural principle for high nuclearity gold clusters. *J Chem Soc Chem Commun* 4:248–250
40. Briant CE, Hall KP, Mingos DMP, Wheeler AC (1986) Synthesis and structural characterisation of hexakis(triphenyl phosphine)hexagold(2+) nitrate, $[\text{Au}_6(\text{PPh}_3)_6][\text{NO}_3]_2$, and related clusters with edgesharing bitetrahedral geometries. *J Chem Soc Dalton Trans* 3: 687–692
41. Cheetham GMT, Harding MM, Haggitt JL, Mingos DMP, Powell HR (1993) Synthesis and microcrystal structure determination of $[\text{Au}_{10}(\text{PPh}_3)_7\{\text{S}_2\text{C}_2(\text{CN})_2\}_2]$ with monochromatic synchrotron radiation. *J Chem Soc Chem Commun* 12:1000–1001
42. Copley RCB, Mingos DMP (1996) The novel structure of the $[\text{Au}_{11}(\text{PMePh}_2)_{10}]^{3+}$ cation: crystal structures of $[\text{Au}_{11}(\text{PMePh}_2)_{10}][\text{C}_2\text{B}_9\text{H}_{12}]_3 \cdot 4\text{thf}$ and $[\text{Au}_{11}(\text{PMePh}_2)_{10}][\text{C}_2\text{B}_9\text{H}_{12}]_3(\text{thf} = \text{tetrahydrofuran})$. *J Chem Soc Dalton Trans* 4:479–489
43. Copley RCB, Mingos DMP (1996) Synthesis and characterization of the centred icosahedral cluster series $[\text{Au}_9\text{MIB}_4\text{Cl}_4(\text{PMePh}_2)_8][\text{C}_2\text{B}_9\text{H}_{12}]$, where MIB=Au, Ag or Cu. *J Chem Soc Dalton Trans* 4:491
44. Cariati F, Naldini L, Simonetta G, Malatesta L (1967) Clusters of gold compounds with 1,2Bis(diphenylphosphino)ethane. *Inorg Chim Acta* 1:315–318
45. Albano VG, Bellon PL, Manasser M, Sansoni M (1970) Intermetallic pattern in metal-atom clusters – structural studies on $\text{Au}_{11}\text{X}_3(\text{PR}_3)_7$ Species. *J Chem Soc D Chem Commun* (18):1210–1211
46. Cariati F, Naldini L (1971) Trianionoeptakis(triarylphosphine)undecagold cluster compounds. *Inorg Chim Acta* 5:172–174

47. Bellon P, Manassero M, Sansoni M (1972) Crystal and molecular structure of tri-iodoheptakis (tri-*p*-fluorophenylphosphine)undecagold. *J Chem Soc Dalton Trans* 14:1481–1487
48. Bellon P, Manassero M, Sansoni M (1973) An octahedral gold cluster: crystal and molecular structure of hexakis[tris-(*p*-tolyl)phosphine]-octahedro-hexagold bis(tetraphenylborate). *J Chem Soc Dalton Trans* 22:2423–2427
49. Manassero M, Naldini L, Sansoni M (1979) A new class of gold cluster compounds. Synthesis and X-ray structure of the octakis(triphenylphosphinegold) dializarinsulphonate, $[\text{Au}_8(\text{PPh}_3)_8](\text{aliz})_2$. *J Chem Soc Chem Commun* (9):385–386
50. Mingos DMP (1983) Polyhedral skeletal electron pair approach. A generalised principle for condensed polyhedra. *J Chem Soc Chem Commun* (12):706
51. Mingos DMP, Snee T, Zhenyang L (1990) Bonding models for ligated and bare clusters. *Chem Rev* 90(2):383–402
52. Wales DJ (2005) Electronic structure of clusters. *Encyclopedia Inorg Chem*. doi:10.1002/9781119951438.eibc0066
53. Schwerdtfeger P (2003) Gold goes nano—from small clusters to low-dimensional assemblies. *Angew Chem Int Ed* 42(17):1892–1895
54. Schmid G (2008) Ionically cross-linked gold clusters and gold nanoparticles. *Angew Chem Int Ed* 47(19):3496–3498
55. Schmid G (2008) The relevance of shape and size of Au_{55} clusters. *Chem Soc Rev* 37(9):1909–1930
56. Yam V, Cheng E (2008) Highlights on the recent advances in gold chemistry—a photophysical perspective. *Chem Soc Rev* 37(9):1806–1813
57. Koshevoy I, Chang Y-C, Karttunen A, Selivanov S, Jänis J, Haukka M, Pakkanen T, Tunik S, Chou P-T (2012) Intensely luminescent homoleptic alkynyl decanuclear gold(I) clusters and their cationic octanuclear phosphine derivatives. *Inorg Chem* 51(13):7392–7403
58. Mingos DMP, Watson MJ (1992) Heteronuclear gold cluster compounds. *Adv Inorg Chem* 39:327–399
59. Teo BK, Zhang H (1995) Polyicosahedrality: icosahedron to icosahedron of icosahedra growth pathway for bimetallic (Au–Ag) and trimetallic (Au–Ag–M; M=Pt, Pd, Ni) supraclusters; synthetic strategies, site preference, and stereochemical principles. *Coord Chem Rev* 143:611–636
60. Schmidbaur H, Schier A (2012) Auophilic interactions as a subject of current research: an up-date. *Chem Soc Rev* 41(1):370–412
61. Schulz-Dobrick M, Jansen M (2006) Supramolecular intercluster compounds consisting of gold clusters and Keggin anions. *Eur J Inorg Chem* 2006(22):4498–4502
62. Wen F, Englert U, Gutrath B, Simon U (2008) Crystal structure, electrochemical and optical properties of $[\text{Au}_9(\text{PPh}_3)_8](\text{NO}_3)_3$. *Eur J Inorg Chem* 2008(1):106–111
63. Cariati F, Naldini L, Simonetta G, Malatesta L (1967) Ethyldiphenylphosphine-gold derivatives with intermetallic bonds. *Inorg Chim Acta* 1:24–26
64. Bartlett PA, Bauer B, Singer SJ (1978) Synthesis of water-soluble undecagold cluster compounds of potential importance in electron microscopic and other studies of biological systems. *J Am Chem Soc* 100(16):5085–5089
65. Gutrath BS, Englert U, Wang Y, Simon U (2013) A missing link in undecagold cluster chemistry: single-crystal X-ray analysis of $[\text{Au}_{11}(\text{PPh}_3)_7\text{Cl}_3]$. *Eur J Inorg Chem* 2013(12):2002–2006
66. Wan X-K, Lin Z-W, Wang Q-M (2012) Au_{20} nanocluster protected by hemilabile phosphines. *J Am Chem Soc* 134(36):14750–14752
67. Schmid G, Pfeil R, Boese R, Bandermann F, Meyer S, Calis GHM, van der Velden JWA (1981) $\text{Au}_{55}[\text{P}(\text{C}_6\text{H}_5)_3]_{12}\text{Cl}_6$ – ein Goldcluster ungewöhnlicher Größe. *Chem Ber* 114(11):3634–3642
68. Bertino M, Sun Z-M, Zhang R, Wang L-S (2006) Facile syntheses of monodisperse ultrasmall Au clusters. *J Phys Chem B* 110(43):21416–21418
69. Kamei Y, Shichibu Y, Konishi K. unpublished results

70. Golightly JS, Gao L, Castleman AW, Bergeron DE, Hudgens JW, Magyar RJ, Gonzalez CA (2007) Impact of swapping ethyl for phenyl groups on diphosphine-protected undecagold. *J Phys Chem C* 111
71. Yanagimoto Y, Negishi Y, Fujihara H, Tsukuda T (2006) Chiroptical activity of BINAP-stabilized undecagold clusters. *J Phys Chem B* 110(24):11611–11614
72. Andreiadis E, Vitale M, Mézailles N, Le Goff X, Le Floch P, Toullec P, Michelet V (2010) Chiral undecagold clusters: synthesis, characterization and investigation in catalysis. *Dalton Trans* 39(44):10608–10616
73. Chen J, Zhang QF, Bonaccorso TA, Williard PG, Wang LS (2014) Controlling gold nanoclusters by diphosphine ligands. *J Am Chem Soc* 136(1):92–95
74. Shichibu Y, Kamei Y, Konishi K (2012) Unique [core+two] structure and optical property of a dodeca-ligated undecagold cluster: critical contribution of the exo gold atoms to the electronic structure. *Chem Commun* 48(61):7559–7561
75. Shichibu Y, Konishi K (2010) HCl-induced nuclearity convergence in diphosphine-protected ultrasmall gold clusters: a novel synthetic route to “magic-number” Au₁₃ clusters. *Small* 6(11):1216–1220
76. Shichibu Y, Suzuki K, Konishi K (2012) Facile synthesis and optical properties of magic-number Au₁₃ clusters. *Nanoscale* 4(14):4125–4129
77. Ito H, Saito T, Miyahara T, Zhong C, Sawamura M (2009) Gold(I) hydride intermediate in catalysis: dehydrogenative alcohol silylation catalyzed by gold(I) complex. *Organometallics* 28(16):4829–4840
78. Teo BK, Shi X, Zhang H (1992) Pure gold cluster of 1:9:9:1:9:9:1 layered structure: a novel 39-metal-atom cluster [(Ph₃P)₁₄Au₃₉Cl₆]Cl₂ with an interstitial gold atom in a hexagonal antiprismatic cage. *J Am Chem Soc* 114(7):2743–2745
79. Das A, Li T, Nobusada K, Zeng Q, Rosi N, Jin R (2012) Total structure and optical properties of a phosphine/thiolate-protected Au₂₄ nanocluster. *J Am Chem Soc* 134(50):20286–20289
80. Strähle J (1995) Synthesis of cluster compounds by photolysis of azido complexes. *J Organomet Chem* 488(1–2):15–24
81. Kamei Y, Shichibu Y, Konishi K (2011) Generation of small gold clusters with unique geometries through cluster-to-cluster transformations: octanuclear clusters with edge-sharing gold tetrahedron motifs. *Angew Chem Int Ed Engl* 50(32):7442–7445
82. Laguna A, Laguna M, Gimeno MC, Jones PG (1992) Synthesis and X-ray characterization of the neutral organometallic gold cluster [Au₁₀(C₆F₅)₄(PPh₃)₅]. *Organometallics* 11(8):2759–2760
83. Vollenbroek FA, Bour JJ, Trooster JM, van der Velden JWA (1978) Reactions of gold? Phosphine cluster compounds. *J Chem Soc Chem Commun* 21:907
84. Nunokawa K, Onaka S, Ito M, Horibe M, Yonezawa T, Nishihara H, Ozeki T, Chiba H, Watase S, Nakamoto M (2006) Synthesis, single crystal X-ray analysis, and TEM for a single-sized Au₁₁ cluster stabilized by SR ligands: the interface between molecules and particles. *J Organomet Chem* 691(4):638–642
85. Shichibu Y, Negishi Y, Watanabe T, Chaki NK, Kawaguchi H, Tsukuda T (2007) Biicosahedral Gold Clusters [Au₂₅(PPh₃)₁₀(SC_nH_{2n+1})₅Cl₂]²⁺ (n = 2–18): a Stepping stone to cluster-assembled materials. *J Phys Chem C* 111(22):7845–7847
86. Yang Y, Sharp PR (1994) New gold clusters [Au₈L₆](BF₄)₂ and [(AuL)₄](BF₄)₂ (L=P (mesityl)₃). *J Am Chem Soc* 116(15):6983–6984
87. Ramamoorthy V, Wu Z, Yi Y, Sharp PR (1992) Preparation and decomposition of gold (I) hydrazido complexes: gold cluster formation. *J Am Chem Soc* 114(4):1526–1527
88. Schulz-Dobrick M, Jansen M (2007) Characterization of gold clusters by crystallization with polyoxometalates: the intercluster compounds [Au₉(dppe)₄][Mo₈O₂₆], [Au₉(dppe)₄][PW₁₂O₄₀] and [Au₁₁(PPh₃)₈Cl₂]₂[W₆O₁₉]. *Z Anorg Allg Chem* 633(13–14):2326–2331
89. Schulz-Dobrick M, Jansen M (2008) Intercluster compounds consisting of gold clusters and fullerides: [Au₇(PPh₃)₇]C₆₀ × THF and [Au₈(PPh₃)₈](C₆₀)₂. *Angew Chem Int Ed Engl* 47(12):2256–2259

90. Gutrath B, Oppel I, Presly O, Beljakov I, Meded V, Wenzel W, Simon U (2013) $[\text{Au}_{14}(\text{PPh}_3)_8(\text{NO}_3)_4]$: an example of a new class of $\text{Au}(\text{NO}_3)$ -ligated superatom complexes. *Angew Chem Int Ed* 52(12):3529–3532
91. Kobayashi N, Kamei Y, Shichibu Y, Konishi K (2013) Protonation-induced chromism of pyridylethynyl-appended [core+exo]-type Au clusters. Resonance-coupled electronic perturbation through pi-conjugated group. *J Am Chem Soc* 135(43):16078–16081
92. Van der Linden JGM, Paulissen MLH, Schmitz JEJ (1983) Electrochemical reduction of the gold cluster $\text{Au}_9(\text{PPh}_3)_8^{3+}$. Evidence for an ErErCr mechanism. Formation of the paramagnetic gold cluster $\text{Au}_9(\text{PPh}_3)_8^{2+}$. *J Am Chem Soc* 105(7):1903–1907
93. Smirnova ES, Echavarren AM (2013) A hexanuclear gold cluster supported by three-center-two-electron bonds and aurophilic interactions. *Angew Chem Int Ed Engl* 52(34):9023–9026
94. Marsh RE (1984) Crystal structure of $\text{Au}_7(\text{PPh}_3)^{7+}$: corrigendum. *Inorg Chem* 23(22):3682–3682
95. Schulz-Dobrick M, Jansen M (2008) Synthesis and characterization of intercluster compounds consisting of various gold clusters and differently charged kegglin anions. *Z Anorg Allg Chem* 634(15):2880–2884
96. Bhargava S, Kitadai K, Masashi T, Drumm DW, Russo SP, Yam VW, Lee TK, Wagler J, Mirzadeh N (2012) Synthesis and structures of cyclic gold complexes containing diphosphine ligands and luminescent properties of the high nuclearity species. *Dalton Trans* 41(16):4789–4798
97. Pethe J, Strähle J (1999) Synthese und Kristallstruktur von $[\text{Au}(\text{AuNCO})(\text{AuPPh}_3)_8]$ Cl. *Z Naturforsch B* 54(3):381–384
98. Pethe J, Maichle-Mössmer C, Strähle J (1998) Synthese und Struktur von $\text{K}[\text{Au}(\text{AuCl})(\text{AuPPh}_3)_8](\text{PF}_6)_2$. *Z Anorg Allg Chem* 624(7):1207–1210
99. Nunokawa K, Onaka S, Yamaguchi T, Ito T, Watase S, Nakamoto M (2003) Synthesis and characterization of the Au_{11} cluster with sterically demanding phosphine ligands by single crystal X-ray diffraction and XPS spectroscopy. *Bull Chem Soc Jpn* 76(8):1601–1602
100. Scherbaum F, Grohmann A, Huber B, Krüger C, Schmidbaur H (1988) “Aurophilicity” as a consequence of relativistic effects: the hexakis(triphenylphosphaneaurio)methane dication $[(\text{Ph}_3\text{PAu})_6\text{C}]^{2\oplus}$. *Angew Chem Int Ed Engl* 27(11):1544–1546
101. Shichibu Y, Konishi K (2013) Electronic properties of [core+exo]-type gold clusters: factors affecting the unique optical transitions. *Inorg Chem* 52(11):6570–6575
102. Jaw HRC, Mason WR (1991) Magnetic circular dichroism spectra for the octakis(triphenylphosphino)nonagold(3+) ion. *Inorg Chem* 30(2):275–278

Gold Clusters, Colloids and Nanoparticles I

Mingos, D.M.P. (Ed.)

2014, IX, 282 p. 137 illus., 90 illus. in color., Hardcover

ISBN: 978-3-319-07847-2